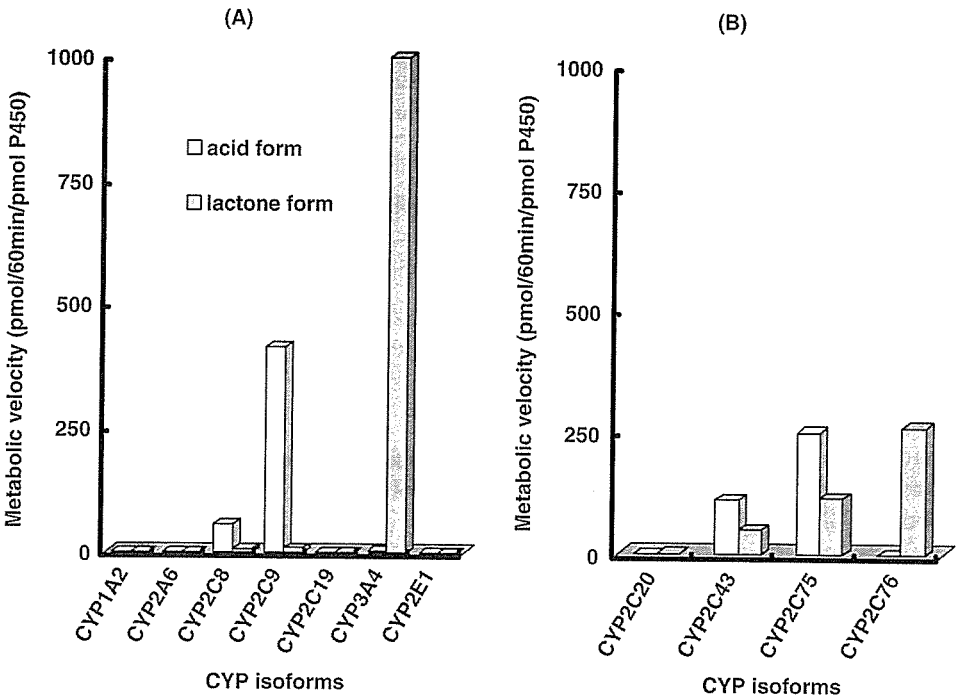

Figure 3. Identification of CYPs involved in pitavastatin metabolism in humans (A) and monkeys (B). Recombinant monkey CYP2C proteins were expressed in *E. coli* and the metabolic assays were performed using the monkey or human CYP proteins as described in the Materials and methods section. Results are based on duplicate determinations.

Table V. Kinetic constants of pitavastatin metabolism in monkey hepatic microsomes and the recombinant proteins for monkey CYP2Cs.

Pitavastatin	Enzyme	Metabolite	Km (μM)	V_{max}* (pmol min^{-1} nmol^{-1} P450)
Acid form	Hepatic microsomes	M-13	13.5	106.7
		M-14	13.4	81.1
	CYP2C43	M-13	129.1	1809
	CYP2C75	M-13	8.8	257.7
		M-14	1.2	7.7
Lactone form	CYP2C75	M-13	7.1	23.5
	CYP2C76	M-3	4.5	96.4
		M-13	24.9	129.1
		M-14	36.6	26.9

*V_{max} for hepatic microsomes is expressed as pmol min^{-1} mg^{-1} protein. Data are derived from duplicate determinations.

Discussion

Monkey CYP2C76, which does not have an orthologue in humans, has metabolic properties different from other monkey CYP2Cs such as CYP2C20, CYP2C43 and

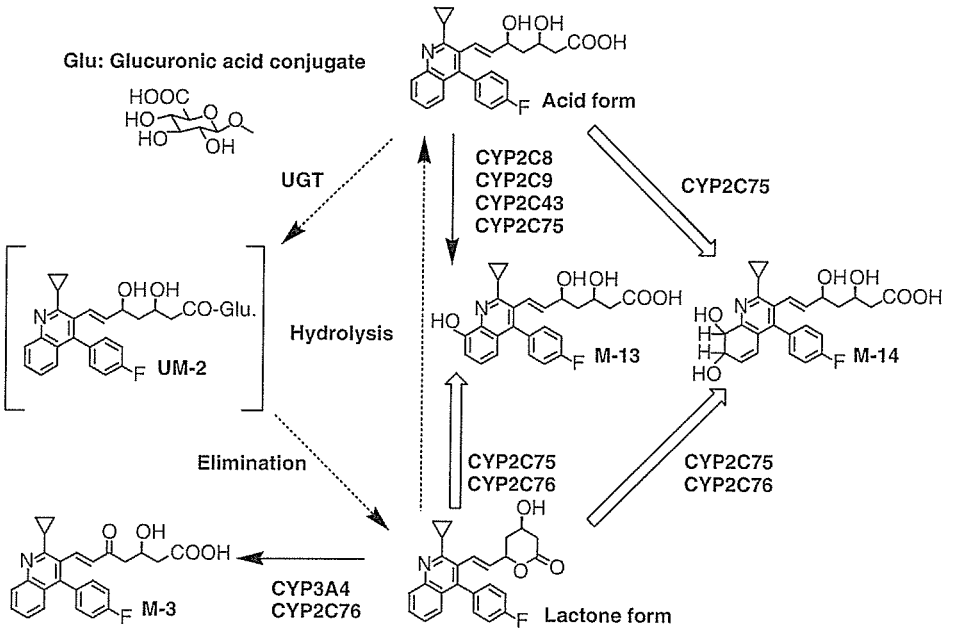

Figure 4. Postulated metabolic pathways of pitavastatin in monkeys and humans. Solid lines indicate common metabolic pathways and dotted lines are the CYP-independent metabolic pathways in monkeys and humans. The block lines indicate the monkey-specific pathways of pitavastatin metabolism.

CYP2C75 (Uno et al. 2006). This species specificity and functional uniqueness strongly suggests that CYP2C76 could be responsible for the some difference in drug metabolism between monkeys and humans. The current study first investigated whether CYP2C76 accounts for the species difference in the metabolism of model substrates for human CYP2Cs. The involvement of CYP2C76, however, could not be clearly indicated for species differences seen in tolbutamide or *S*-mephenytoin metabolism between monkeys and humans. Therefore, we decided to investigate pitavastatin metabolism, in which the different metabolic processes have been noted for the acid and lactone forms in monkeys as compared to humans.

CYP2Cs are substantially involved in pitavastatin metabolism, as evidenced by inhibition studies. Anti-CYP2C9 antisera showed a potent inhibition, whereas chemical inhibitors specific for human CYP2C8/9 such as quercetin, sulphafenazole and gemfibrozil, did not inhibit the metabolism of either form in monkey hepatic microsomes. These results indicate that monkey CYP2Cs play an important role in pitavastatin metabolism; however, differences exist in site- or substrate-selectivity for the activities of CYP2Cs between monkeys and humans. On the other hand, a substantial inhibition of the acid form was noted in the presence of tranylcypromine, a human CYP2C19 inhibitor. Moreover, benzoflavone and ketoconazole, which selectively inhibit human CYP1A2 and CYP3A4, respectively, showed a potent inhibition for the lactone form. These results suggest that different CYP2Cs are involved in the metabolism of each form of pitavastatin.

Analysis using recombinant proteins also indicated the involvement of CYP2Cs in pitavastatin metabolism in monkeys, namely CYP2C75 and CYP2C76, but not CYP2C20. Moreover, the metabolic properties mediated by these monkey CYP2Cs exhibited a substantial difference in metabolite formation and metabolic clearance of pitavastatin as compared with those of human CYP2Cs. As proposed in Figure 4, monkey CYP2C75 is

critically involved in the overall formation of M-13 and M-14 with relatively low K_m values. CYP2C76 is mainly involved in the metabolism of the lactone form to generate M-3, M-13 and M-14. In other species, the lactone form is metabolized by CYP3As such as CYP3A4 in humans, CYP3A2 in rats, or CYP3A12 in dogs (data not shown). These results clearly indicate that CYP2C76 is involved in the species difference of pitavastatin metabolism between monkeys and humans.

Considering the apparent involvement of CYP2C76 in the species difference between monkeys and humans in drug metabolism, identification and characterization of monkey CYPs responsible for drug metabolism are an inevitable task to better understand species difference between monkeys and humans. The unidentified species–specific CYPs other than CYP2C76, if any, could also result in the difference of in drug metabolism between monkeys and humans. Two different CYP2Ds in common marmosets, CYP2D19 and CYP2D30, show different metabolic properties, although it is not known whether these CYP2Ds are encoded by different genes (Hichiya et al. 2004). Based on this report, it was considered that these CYP2Ds, if present in the genome as distinct genes, could be responsible for species differences between monkeys and humans, considering that only CYP2D6 is functional among the three human CYP2D genes identified to date. The evolutionary closeness of cynomolgus monkeys to common marmosets raises the possibility that cynomolgus monkeys might also have more than one CYP2D6-related protein. By immunoblotting studies, two distinct protein bands were detected which are immuno-reactive with human CYP2D6 antibodies in cynomolgus monkey liver (Weaver et al. 1999), making this possibility more likely.

Eliminating the function of CYP2C76 in monkeys is expected to lead to a metabolic pattern even more similar to humans. Inactivation of the gene itself has been accomplished by gene-targeting in mice, but has not been successfully applied to non-human primate species including cynomolgus monkeys (Norgren, 2004). An alternative way is to identify functionally null or defective mutations, which have been reported for the human CYP genes including CYP2C8, CYP2C9, CYP2C19 (for details, see http://www.imm.ki.se/CYPalleles/). Similar mutations were also identified in dogs, which are frequently used in the preclinical studies of drug metabolism. A nonsense mutation (C1117T) in CYP1A2 decreases the production of the intact protein, leading to the phenotype of poor metabolizer (Mise et al. 2004). Moreover, >10% of 149 beagle dogs analysed were homozygotes for this mutation (Tenmizu et al. 2004). With the relatively high frequency of such defective or null alleles, such alleles might be easily identified in CYP2C76 and utilized to establish better model animals homozygous with the alleles in monkeys.

In conclusion, we have provided evidence that CYP2C76 is responsible for the species difference in the metabolism of pitavastatin. Using monkey CYP2C recombinant proteins, further investigations will elucidate the involvement of CYP2C76 for species difference between monkeys and humans in CYP2C-dependent metabolism of various drugs. Further identification and characterization of monkey-specific drug-metabolizing enzymes should help to understand more fully species difference in drug metabolism between monkeys and humans and to extrapolate the data obtained using monkeys to humans.

Acknowledgements

The authors are grateful to Mr Junji Kojima, Mr Tsuyoshi Saito and Mr Shin-ichiro Ogawa for their technical assistant and invaluable suggestions.

References

Aoki T, Yoshinaka Y, Yamazaki H, Suzuki H, Tamaki T, Sato F, Kitahara M, Saito Y. 2002. Triglyceride-lowering effect of pitavastatin in a rat model of postprandial lipemia. European Journal of Pharmacology 444:107–113.

Bogaards JJP, Bertrand M, Jackson P, Oudshoorn MJ, Weaver RJ, Bladeren PJ, Walther B. 2000. Determining the best animal model for human cytochrome P450 activities: A comparison of mouse, rat, rabbit, dog, micropig, monkey and man. Xenobiotica 12:1131–1152.

Daigo S, Takahashi Y, Fujieda M, Ariyoshi N, Yamazaki H, Koizumi W, Tanabe S, Saigenji K, Nagayama S, Ikeda K, Nishioka Y, Kamataki T. 2002. A novel mutant allele of the CYP2A6 gene (CYP2A6*11) found in a cancer patient who showed poor metabolic phenotype towards tegafur. Pharmacogenetics 12:299–306.

Fujino H, Kojima J, Yamada Y, Kanda H, Kimata H. 1999a. Studies on the metabolic fate of NK-104, a new inhibitor of HMG-CoA reductase (4): Interspecies variation in laboratory animals and humans. Xenobiotic Metabolism and Disposition 14:79–91.

Fujino H, Saito T, Tsunenari Y, Kojima J, Sakaeda T. 2004b. Metabolic properties of the acid form and lactone form of HMG-CoA reductase inhibitors. Xenobiotica 34:961–971.

Fujino H, Saito T, Tsunenari Y, Kojima J. 2004a. Effect of gemfibrozil on the metabolism of pitavastatin – Determining the best animal model for human CYP and UGT activities. Drug metabolism and Drug Interactions 20:25–42.

Fujino H, Yamada I, Hirano M, Yoneda M. 1999b. Studies on the metabolic fate of NK-104, a new inhibitor of HMG-CoA reductase (5): In vitro metabolism and plasma protein binding in animals and human. Xenobiotic Metabolism and Disposition 14:415–424.

Fujino H, Yamada I, Shimada S, Yoneda M, Kojima J. 2003. Metabolic fate of pitavastatin, a new inhibitor of HMG-CoA reductase: Human UDP-glucuronosyltransferase enzymes involved in lactonization. Xenobiotica 33:27–41.

Fujino H, Yamada I, Shimada S, Yoneda M. 2001. Simultaneous determination of taxol and its metabolites in microsomal samples by a simple thin-layer chromatography radioactivity assay. Journal of Chromatography 757:143–150.

Hichiya H, Kuramoto S, Yamamoto S, Shinoda S, Hanioka N, Narimatsu S, Asaoka K, Miyata A, Iwata S, Nomoto M, Satoh T, et al. 2004. Cloning and functional expression of a novel marmoset cytochrome P450 2D enzyme, CYP2D30: Comparison with the known marmoset CYP2D19. Biochemical Pharmacology 68:165–175.

Iwata H, Fujita K, Kushida H, Suzuki A, Konno Y, Nakamura K, Fujino A, Kamataki T. 1998. High catalytic activity of human cytochrome P450 co-expressed with human NADPH-cytochrome P450 reductase in Escherichia coli. Biochemical Pharmacology 55:1315–1325.

Jacqz E, Billante C, Moysan F, Mathieu H. 1988. The non-human primate: A possible model for human genetically determined polymorphisms in oxidative drug metabolism. Molecular Pharmacology 34:215–217.

Kimata H, Fujino H, Koide T, Yamada Y, Tsunenari Y, Yonemitsu M. 1998. Studies on the metabolic fate of NK-104, a new inhibitor of HMG-CoA reductase (1): Absorption, distribution, metabolism and excretion in rats. Xenobiotic Metabolism and Disposition 13:484–498.

Kojima J, Fujino H, Yosimura M, Morikawa H, Kimata H. 1999. Simultaneous determination of NK-104 and its lactone in biological samples by column-switching high-performance liquid chromatography with ultraviolet detection. Journal of Chromatography (B) 724:173–180.

Komori M, Kikuchi O, Sakuma T, Funaki J, Kitada M, Kamataki T. 1992. Molecular cloning of monkey liver cytochrome P-450 cDNAs: Similarity of the primary sequences to human cytochromes P-450. Biochimica et Biophysica Acta 1171:141–146.

Ludwig E, Wolfinger H, Ebner T. 1998. Assessment of microsomal tolbutamide hydroxylation by a simple thin-layer chromatography radioactivity assay. Journal of Chromatography 707:347–350.

Matsunaga T, Ohmori S, Ishida M, Sakamoto Y, Nakasa H, Kitada M. 2002. Molecular cloning of monkey CYP2C43 cDNA and expression in yeast. Drug Metabolism and Pharmacokinetics 17:117–124.

Mise M, Hashizume T, Matsumoto S, Terauchi Y, Fujii T. 2004. Identification of non-functional allelic variant of CYP1A2 in dogs. Pharmacogenetics 14:769–773.

Narimatsu S, Kobayashi N, Masubuchi Y, Horie T, Kakegawa T, Kobayashi H, Hardwick JP, Gonzalez FJ, Shimada N, Ohmori S, Kitada M, et al. 2000. Species difference in enantioselectivity for the oxidation of propranolol by cytochrome P450 2D enzymes. Chemico-Biological Interactions 15:73–90.

Nedelcheva V, Gut I. 1994. P450 in the rat and man: Methods of investigation, substrate specificities and relevance to cancer. Xenobiotica 24:1151–1175.

Norgren Jr RB. 2004. Creation of non-human primate neurogenetic disease models by gene targeting and nuclear transfer. Reproductive Biology and Endocrinology 2:40.

Ohi H, Toratani S, Komori M, Miura T, Kitada M, Kamataki T. 1989. Comparative study of cytochrome P-450 in liver microsomes. A form of monkey cytochrome P-450, P-450-MK1, immunochemically cross-reactive with antibodies to rat P-450-male. Biochemical Pharmacology 38:361–365.

Prueksaritanont T, Gorham LM, Hochman JH, Tran LO, Vyas KP. 1996. Comparative studies of drug-metabolizing enzymes in dog, monkey, and human small intestines, and in Caco-2 cells. Drug Metabolism and Disposition 24:634—642.

Sharer JE, Shipley LA, Vandenbranden MR, Binkley SN, Wrighton SA. 1995. Comparisons of phase one and phase two in vitro hepatic enzyme activities of human, dog, rhesus monkey, and cynomolgus monkey. Drug Metabolism and Disposition 23:1231–1241.

Stevens JC, Shipley LA, Cashman JR, Vandenbranden M, Wrighton SA. 1993. Comparison of human and rhesus monkey in vitro phase I and phase II hepatic drug metabolism activities. Drug Metabolism and Disposition 21:753–760.

Suzuki H, Aoki T, Tamaki T, Sato F, Kitahara M, Saito Y. 1999. Hypolipidemic effect of NK-104, a potent HMG-CoA reductase inhibitor, in guinea pigs. Atherosclerosis 146:259–270.

Tenmizu D, Endo Y, Noguchi K, Kamimura H. 2004. Identification of the novel canine CYP1A2 1117C > T SNP causing protein deletion. Xenobiotica 34:835–846.

Uno Y, Fujino H, Kito G, Kamataki T, Nagata R. 2006. CYP2C76, a novel CYP in cynomolgus monkey, is a major CYP2C in liver, metabolizing tolbutamide and testosterone. Molecular Pharmacology 70:477–486.

Weaver RJ, Dickins M, Burke MD. 1999. A comparison of basal and induced hepatic microsomal cytochrome P450 monooxygenase activities in the cynomolgus monkey (Macaca fascicularis) and man. Xenobiotica 29:467–482.

Weaver RJ, Thompson S, Smith G, Dickins M, Elcombe CR, Mayer RT, Burke MD. 1994. A comparative study of constitutive and induced alkoxyresorufin O-dealkylation and individual cytochrome P450 forms in cynomolgus monkey (Macaca fascicularis), human, mouse, rat and hamster liver microsomes. Biochemical Pharmacology 47:763–773.

Yamada I, Fujino H, Shimada S, Kojima J. 2003. Metabolic fate of pitavastatin, a new inhibitor of HMG-CoA reductase: Similarities and difference in the metabolism of pitavastatin in monkeys and humans. Xenobiotica 33:789–803.

Available online at www.sciencedirect.com
ScienceDirect
Molecular Genetics and Metabolism 90 (2007) 58–63
Molecular Genetics and Metabolism
www.elsevier.com/locate/ymgme

Stop codon mutations in the flavin-containing monooxygenase 3 (*FMO3*) gene responsible for trimethylaminuria in a Japanese population

Hiroshi Yamazaki [a,b,*], Haruka Fujita [a], Takaaki Gunji [b], Jun Zhang [c], Tetsuya Kamataki [b], John R. Cashman [c], Makiko Shimizu [a]

[a] *Laboratory of Drug Metabolism and Pharmacokinetics, Showa Pharmaceutical University, Machida, Tokyo 194-8543, Japan*
[b] *Graduate School of Pharmaceutical Sciences, Hokkaido University, Sapporo 060-0812, Japan*
[c] *Human BioMolecular Research Institute, San Diego, CA 92121, USA*

Received 15 June 2006; received in revised form 11 August 2006; accepted 11 August 2006
Available online 25 September 2006

Abstract

The reduced capacity of flavin-containing monooxygenase 3 (FMO3) to *N*-oxidize trimethylamine (TMA) is believed to cause a metabolic disorder. The aim of this study was to investigate the inter-individual variations of FMO3. Genomic DNA of case subjects that showed only 10–20% of FMO3 metabolic capacity among self-reported trimethylaminuria Japanese volunteers was sequenced. Functional analysis of recombinant FMO3 proteins was also performed. One homozygote for a novel single nucleotide substitution causing a stop codon at Arg500 was observed. The biological parents of this Proband A were heterozygous and showed >90% TMA *N*-oxygenation metabolic capacity. Another Proband B had the Arg500Stop and Cys197Stop codons. The TMA *N*-oxygenation metabolic capacities of the father and brother of this Proband B were apparently observed by possessing Arg205Cys mutant that coded for decreased TMA *N*-oxygenase. Recombinant Arg500Stop FMO3 cDNA expressed in *Escherichia coli* membranes and a series of highly purified truncation mutants at different positions of the C-terminus of FMO3 showed no detectable functional activity toward typical FMO3 substrates. The results suggest that individuals homozygous for either of the nonsense mutations, Arg500Stop and/or Cys197Stop alleles, in the *FMO3* gene can possess abnormal TMA *N*-oxygenation.

Keywords: Flavin-containing monooxygenase; Fish-like odor syndrome; Trimethylamine; Truncated FMO3; Japanese; Trimethylaminuria

Introduction

The flavin-containing monooxygenase (FMO, EC 1.14.13.8) is an NADPH-dependent enzyme that catalyzes the oxygenation of a wide variety of nucleophilic compounds containing sulfur, nitrogen or phosphorus atoms [1,2]. To date, eleven *FMO* genes have been identified in humans (*FMO1* to *FMO11p*) but only FMO1–5 are functionally active [3]. FMO3 is considered a prominent functional form expressed in adult human liver although FMO5 is also present [4,5]. In humans, a 20-fold inter-individual variation in FMO3 expression levels have been reported [6,7]. FMO3 may also play a role in processing some types of drugs such as the anticancer drug tamoxifen, the pain medication codeine, the antifungal drug ketoconazole, the addictive chemical nicotine found in tobacco, and diet-derived trimethylamine (TMA) [1,2]. Wild-type human FMO3 has 532 amino acids but there are genetic polymorphisms in the *FMO3* gene that code for naturally truncated forms that have no or almost no detectable amount of functional enzymatic activity [1,8–10]. Mutations in the *FMO3* gene are summarized in a Web-database using systematic and trivial names [8].

* Corresponding author. Fax: +81 42 721 1406.
E-mail address: hyamazak@ac.shoyaku.ac.jp (H. Yamazaki).

1096-7192/$ - see front matter © 2006 Elsevier Inc. All rights reserved.
doi:10.1016/j.ymgme.2006.08.008

Trimethylaminuria, or fish-like odor syndrome, is a genetic disease characterized by excretion of excessive unmetabolized TMA [11,12]. Individuals suffering from trimethylaminuria have a decreased capacity to oxygenate free malodorous TMA to non-odorous trimethylamine *N*-oxide (TMAO) by the FMO3 [13,14] and this is the case for individuals with causative nonsense *FMO3* gene mutations found in North American and European populations [15,16]. Unpleasant and/or pungent malodor caused by excess TMA present in various bodily fluids of some affected individuals may lead to profound social problems [11,12].

Due to its strong linkage with trimethylaminuria, considerable work has been done related to the contribution of genetic polymorphisms of the *FMO3* gene of the coding region to inter-individual differences in FMO3 phenotype [17–19]. In order to identify novel mutations of FMO3 and/or haplotypes of the *FMO3* gene found in Japanese individuals suffering from trimethylaminuria, we resequenced the entire coding region of the *FMO3* gene using genomic DNA from individuals that, judged by self-reported analysis were suspected to be positive for trimethylaminuria and later showed low FMO3 metabolic capacity on the basis of urine testing of TMAO levels. In a preliminary report [20], there were some FMO3 variants like Cys197Stop, Asp198Glu or Arg205Cys observed in a Japanese population, but the characterization of these FMO3 mutants were not examined in detail.

Herein, we report data supporting the involvement of two novel deleterious *FMO3* gene mutations causative of abnormal TMA *N*-oxygenation and trimethylaminuria in self-reporting Japanese individuals that were diagnosed with low FMO3 metabolic capacity based on urine testing. Subjects homozygous for either of the nonsense mutations, Arg500Stop and Cys197Stop alleles, in the *FMO3* gene suffered from trimethylaminuria.

Materials and methods

Chemicals

TMA and TMAO were obtained from Wako Pure Chemicals (Osaka, Japan). The tertiary amine substrate 10-[(*N*,*N*-dimethylaminopentyl)-2-(trifluoromethyl)]phenothiazene (5-DPT) and its *N*-oxide were synthesized as described previously [1,21]. The other chemicals and reagents used were obtained in the highest grade available commercially.

Subjects

The Ethics Committees of Showa Pharmaceutical University and Hokkaido University approved this study. Volunteer subjects who responded to an Internet article for screening of urinary TMA and TMAO levels and for sequencing the *FMO3* gene included 90 males and 74 females ranging from 1 to 64 years of age. Informed consent was obtained from each subject or parent. The study participants collected their urine samples as described previously [22]. Urinary TMA and TMAO concentrations were determined by gas chromatography using a flame ionization detector as described previously [23]. Urinary concentrations of free TMA or total TMA (μmol/mL of urine) were corrected for creatinine excretion (mmol/mL) [22]. Individuals that showed impaired FMO3 metabolic capacity, defined as the ratio of TMAO to total TMA (% of TMAO/(TMA + TMAO)), lower than 40% were considered to constitute abnormal TMA metabolism and possibly suffering from severe trimethylaminuria [16,22,24]. The values of urinary TMA and TMAO were shown as the average of at least three determinations obtained from first morning void urine.

DNA analysis

Genomic DNA prepared from peripheral lymphocytes [20] or buccal cells [25] of the study participants were analyzed. The sequence of the complete human *FMO3* gene described in GenBank (Accession Number AL021026) was used as a reference. Polymerase chain reaction (PCR) for the all exons and exon–intron junctions of the human *FMO3* gene was conducted in a 25 μL reaction mixture containing 50 ng of genomic DNA, 1.0 U LA-*Taq* DNA polymerase (Takarabio, Shiga, Japan), LA-PCR buffer, 2.0 mM $MgCl_2$, 0.2 mM dNTPs, 5.0 pmol of each sense and antisense primer reported previously [23]. The PCR conditions consisted of an initial denaturation at 94 °C for 1 min, followed by 35 cycles of denaturation at 94 °C for 30 s, annealing at 55 °C for 30 s, and extension at 72 °C for 45 s. The PCR products were directly sequenced on both strands using an ABI bigdye terminator cycle sequencing kit (Applied Biosystems, Foster City, CA, USA) with the sequencing primers [20]. The purified PCR products were analyzed on an ABI PRISM 3730*xl* DNA analyzer (Applied Biosystems).

Genotyping analysis for the novel g.30398 C > T mutation (Arg500Stop FMO3) in exon 9 was also carried out by a PCR-restriction fragment length polymorphism (RFLP) method with amplified DNA with the primers FMO3-9S and FMO3-9AS [23] and digestion by *Bss*SI at 37 °C for 2 h.

Recombinant wild-type and modified FMO3 protein preparations

The FMO3 cDNA used was previously modified by a PCR procedure [23] using a 5′-primer (5′-AAAAAGCTTACCATGGGGAAGAAAG-3′, that introduced an *Nco*I site prior to the start codon) and a 3′-primer (5′-CTAGAGAAGCTTATGATTAGGTCAACAC-3′, that introduced a *Hin*dIII site downstream of the stop codon). The full-length DNA sequence was confirmed again using DNA re-sequencing of both strands. To produce Arg205Cys FMO3, site-directed mutagenesis was performed by the primer-directed enzymatic amplification method [23]. Briefly, G-base at position 706 bp in the FMO3 cDNA was substituted by a T-base using the primers, 5′-AGAACTCAGCtGCACAGCAGA-3′ and 5′-TCTGCTGTGCaGCTGAGTTCT-3′, to introduce the single nucleotide substitution, that coded for Arg205Cys in exon 5. Similarly, a C-base at position 1590 bp was substituted by a T-base for preparation of Arg500Stop FMO3. The resultant cDNAs were amplified by KOD polymerase (Toyobo, Osaka, Japan). The wild-type and modified FMO3 cDNAs were introduced into the pTrc99A expression vector (Pharmacia Biotechnology, Milwaukee, MI, USA) and then transformed into *E. coli* strain JM109 as described previously [23]. The entire coding regions of the wild-type and mutagenized FMO3 cDNAs including the mutated sites were verified by re-sequencing of both strands.

Membrane fractions were prepared from the bacterial pellets that the FMO3 cDNAs had been introduced into by a series of fractionations and high-speed centrifugation steps as described previously [23]. Briefly, *E. coli* JM109 transformed by the FMO3 expression vector was grown overnight at 37 °C in Luria–Bertani medium containing 50 μg/mL ampicillin. A 1.0 mL aliquot of the starter culture was inoculated into 100 mL of Terrific Broth medium containing 50 μg/mL ampicillin, and 100 mM potassium phosphate buffer (pH 7.4) in a 300-mL triple-baffled flask and cultivated at 120 rpm at 30 °C. After the absorbance of the culture broth at a wavelength of 600 nm reached 0.3, 1 mM isopropyl-β-D-thiogalactoside was added and shaking was continued further for 24 h at 30 °C. The cells were then harvested by centrifugation at 10,000*g* for 20 min. All subsequent steps were carried out at 4 °C. The cells were resuspended (*ca.* 0.03 g/mL) in 50 mM Tris–acetate buffer (pH 7.5) containing 0.25 mM EDTA, 0.25 M sucrose, and 0.1 mg/mL lysozyme. The cell suspension was kept on ice for 30 min and then centrifuged at 9000*g* for 10 min. The pellet was resus-

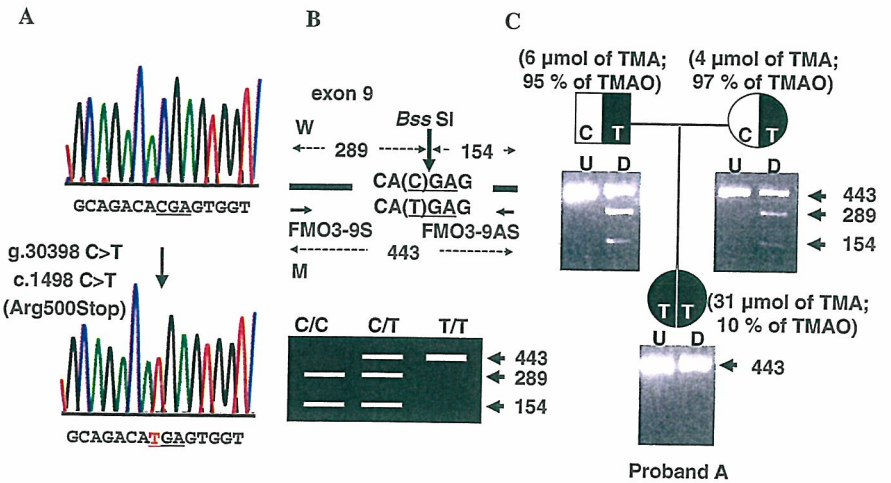

Fig. 1. (A) Nucleotide sequences of wild-type and variant of exon 9 of the *FMO3*. Both strands were sequenced. The sequences are shown only for sense strands for exon 9 of genomic DNA from the Proband A. (B) Genotyping analysis for the novel g.30398 C > T mutation (Arg500Stop FMO3) in exon 9 by PCR-RFLP with *Bss*SI. Genomic DNA was amplified with primers FMO3-9S and FMO3-9AS [23] and was digested by *Bss*SI. (C) Pedigree analysis for the presence of novel Arg500Stop mutation in the *FMO3* gene of the Proband A. The numbers in parentheses showed the results of both free TMA concentration (µmol TMA/mmol creatinine) and FMO3 metabolic capacity (% of TMAO to total TMA + TMAO) from analysis of urine. The PCR products before and after digestion with *Bss*SI were separated on 2 % agarose gel. U, uncut; D, digested with *Bss*SI.

pended (*ca.* 0.5 g/mL) in 100 mM potassium phosphate buffer (pH 7.4) containing 20% (v/v) glycerol, 6 mM magnesium acetate, 0.1 mM dithiothreitol, and 0.1 mM phenylmethylsulfonyl fluoride. Cells were disrupted using an ultrasonic processor and the resulting lysate was centrifuged at 9000*g* for 20 min. The supernatant was then further centrifuged at 100,000*g* for 1 h. The pellet (membrane fraction) was resuspended in one volume of 10 mM Tris–HCl buffer (pH 7.4) containing 0.1 mM EDTA and 20% glycerol (v/v). The amount of recombinant FMO3 was determined by immunoquantification by comparison with a standard of human FMO3 (BD Gentest, Woburn, MA, USA) and by the FAD content [23,26].

Wild-type human FMO3 and several truncated variants were also expressed in *E. coli* as maltose-binding fusion proteins using the expression vector pMAL-c2 [21,27]. The maltose-binding FMO3 proteins were purified by affinity chromatography as described previously [1,21,27].

Other assays

Rates of *N*-oxygenation of TMA and 5-DPT by recombinant FMO3 forms were determined by gas chromatography and HPLC, respectively, as described previously [23,27]. The methods yielded precision and accuracy of <10 % with linearity of time- (to 60 min) or protein- (to 1 mg/mL) dependent manner. The kinetic analysis of TMA *N*-oxygenation was performed using a nonlinear regression analysis program (KaleidaGraph, Synergy Software, Reading, PA, USA).

Results

DNA analysis of Proband A

FMO3 metabolic capacity was determined in self-reporting individuals that claimed to possess defective TMA *N*-oxygenation. Based on a low metabolic capacity of FMO3 (⩽40% urinary TMAO formation) causing severe trimethylaminuria symptoms [16,19], the frequency of subjects that showed less than 40% of FMO3 metabolic capacity was only 3.0% (5 individuals out of 164 individuals) in a Japanese population.

We focused on one of the participants that showed low metabolic capacity for TMA *N*-oxygenation (10–20%). From Proband A who showed 10 % FMO3 metabolic capacity, a single nucleotide substitution at g.30398 C > T in the *FMO3* gene was observed that resulted in c.1498C > T and caused a stop codon at Arg500 in exon 9 (Fig. 1A). The Proband A was homozygous for this novel FMO3 stop codon mutation. To confirm the mutation of this *FMO3* gene, a simple PCR-RFLP method was developed. As shown in Fig. 1B, the PCR product from the Arg500stop codon could not be digested by *Bss*SI. A more extensive analysis of DNA revealed that both parents of Proband A were heterozygous for the mutation at g.30398 C > T (Arg500Stop) (Fig. 1C). Analysis of urinary TMA *N*-oxygenation of both parents showed FMO3 metabolic capacity was greater than 90%, in contrast to 10 % metabolic capacity of Proband A (Fig. 1C).

DNA analysis of Proband B

We also observed the novel Arg500Stop mutation in the *FMO3* gene from Proband B that also possessed 21% metabolic capacity. In the course of sequencing the FMO3 DNA of the samples from this family (Fig. 2), we found that Proband B was heterozygous for the Arg500Stop allele and also had another allele (Fig. 2A) that was reported recently as a single nucleotide polymorphism [20]. The latter *FMO3* mutation was the g.21243_21244 TG deletion (c.591_592TG > del) caused a frameshift that encoded a new stop codon. This *FMO3* allele had g.5906 C > T and g.5907 A > G in intron 2, g.20852 C > T in exon 4 (c.441C > T), a g.20960_20962 CTT deletion, g.21115 G > A in intron 4, g.21246 T > A in exon 5 (c.594T > A), g.27091 C > T in exon 7 (c.855C > T), and a g.29232 T insertion in intron 8, together with the g.21243_21244 TG deletion in exon 5 (c.591_592TG > del) that coded for Cys197Stop.

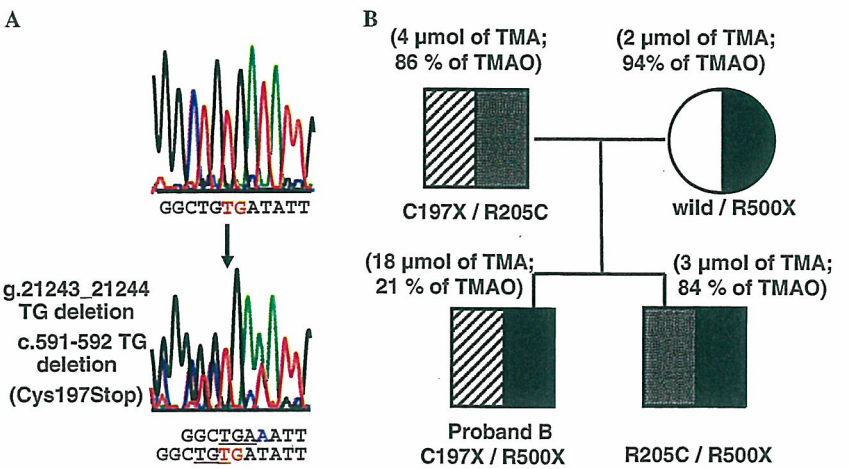

Fig. 2. (A) Nucleotide sequences of wild-type and variant of exon 5 of the *FMO3*. Both strands were sequenced. Antisense stands for exon 5 of genomic DNA from the Proband B are shown in a reversed manner, because of upstream deletions in sense strands. (B) A family study for Proband B who was heterozygous for Cys197Stop and Arg500Stop FMO3 mutations. See legend of Fig. 1 for details.

Other mutations

In addition, we found another haplotype containing g.21265 C>T in exon 5 (c.613C>T) from the father and brother of the Proband B that resulted in Arg205Cys FMO3 [20]. The individuals that were heterozygous for Arg205Cys FMO3 showed 84–86% of the FMO3 metabolic capacity *in vivo* (Fig. 2B). We recently reported two additional missense mutants, Thr201Lys FMO3 and Met260Val FMO3, as a preliminary single nucleotide polymorphism communication [28] from the other three subjects out of 164 individuals showing less than 40% FMO3 metabolic capacities.

The allelic frequencies of Cys197Stop, Arg205Cys, and Arg500Stop of the *FMO3* gene were estimated to be 2.1% (7 out of 328 alleles), 4.0% (13 out of 328 alleles), and 2.7% (9 out of 328 alleles), respectively, in this Japanese cohort. Additional Thr201Lys and Met260Val mutations showed less frequencies estimated to be 1.2% (4 out of 328 alleles) and 0.6% (2 out of 328 alleles), respectively, in the same cohort.

Recombinant Arg205Cys or Arg500Stop FMO3

Kinetic parameters for TMA *N*-oxygenation functional activity were determined by nonlinear regression analysis of recombinant Arg205Cys FMO3 and were compared with those of wild-type FMO3 expressed in bacterial membranes (Table 1). Apparent K_m values of wild-type and Arg205Cys FMO3 were not significantly different, but the V_{max} value of Arg205Cys was approximately one-fourth of that of wild-type enzyme.

To evaluate functional activity of the FMO3 mutant encoding a stop codon, recombinant Arg500Stop FMO3 was expressed in *E. coli* membranes and analyzed for functional activity. The Arg500Stop FMO3 expressed in the membranes was not able to catalyze *N*-oxygenation of TMA or another tertiary amine substrate for FMO3, 5-DPT (Table 2).

Table 1
Trimethylamine *N*-oxygenation activity of wild-type and Arg205Cys FMO3 cDNA expressed in *E. coli*

FMO3	Trimethylamine *N*-oxygenation activity	
	K_m (μM)	V_{max} (nmol products/min/nmol FMO3)
Wild-type	40 ± 8	16 ± 1
Arg205Cys	40 ± 5	4.2 ± 0.5

The *N*-oxygenation of trimethylamine (10–500 μM) was determined by gas chromatography.
Kinetic parameters were calculated from the fitted curve by nonlinear regression (means ± SE).

Table 2
Functional activity of wild-type and Arg500Stop FMO3 cDNA expressed in *E. coli*

FMO3	*N*-Oxygenation activity (nmol products/min/nmol FMO3)	
	Trimethylamine	5-DPT
Wild-type	14.1	2.1
Arg500Stop	<0.1	<0.01

The *N*-oxygenation of trimethylamine (100 μM) and 5-DPT (250 μM) were determined by gas chromatography and HPLC, respectively, in triplicate.
5-DPT, 10-[(*N*,*N*-dimethylaminopentyl)-2-(trifluoromethyl)]phenothiazene.

To further investigate the effects of stop codons on 5-DPT *N*-oxygenation, six highly purified FMO3 fusion proteins truncated at Phe510, Ser467, Leu437, Glu403, Asp339, and Glu305 were also studied. A series of highly purified FMO3 fusion proteins truncated at different positions (from Glu305 to Ser467) did not show any detectable enzymatic activities (<0.01 nmol products/min/nmol FMO3), except for Phe510Stop FMO3 that had *N*-oxygenation functional activity (0.02 nmol products/min/nmol FMO3) that was only 1% that of purified wild-type FMO3 fusion protein. These results collectively suggested that Cys197Stop FMO3 and Arg500Stop FMO3 possessed little

or no detectable functional activity as well, suggesting specific regions of the N-terminus of FMO3 was required for functional activity.

Discussion

The structural organization of the human *FMO3* gene has been reported [29]. Human *FMO3* is the gene candidate considered to be solely responsible for TMA *N*-oxygenation and deoderation and is defective in the inherited disorder, fish-like odor syndrome or trimethylaminuria. Because the functional FAD- and $NADP^+$-binding domains of the human *FMO3* (532 amino acids) are encoded by exon 2 and exon 5, respectively [29], it is possible that mutation(s) located toward the N-terminus of the *FMO3* could be responsible for decreased expression of the gene and/or abnormal functional activity or instability of the encoded protein. Previously, inactive variants of FMO3 at positions in exon 2 and exon 5 have been reported [8,9]. In the present study, a new mutation (Arg205Cys FMO3 in exon 5) was identified that possessed functional activity but decreased TMA *N*-oxygenase activity (Table 1). The frequency of this allelic variation may contribute to mild trimethylaminuria observed in the Japanese population, in association with a loss-of-function mutation on the other allele.

In addition, a novel Arg500Stop mutation (Fig. 1) responsible for severe trimethylaminuria was discovered in the Japanese population of the present study. Arg500Stop FMO3 encodes a 499 amino acid protein (out of 532 amino acids, or only 94% of the whole FMO3 structure). The Proband A that was a homozygote for this novel allele (Fig. 2) did not efficiently *N*-oxygenate dietary-derived TMA to TMAO. The observations about abnormal or impaired TMA *N*-oxygenation based on *in vivo* phenotype caused by the stop codon mutation in the *FMO3* gene was supported by *in vitro* evidence that showed no detectable functional activity of Arg500Stop FMO3 expressed in bacterial membranes (Table 2). Important contribution of C-terminus of human FMO3 for its function was clearly indicated but might be inconsistent with early findings of active recombinant FMO2 form in which the C-terminal 26 amino acids were deleted [30]. A molecular modeling of human FMO3 (532 amino acids) is worth examining to understand the contribution of C-terminus based on the recently reported crystal structure of yeast FMO (447 amino acids) [31], in spite of the low sequence identity (~20%) and short length (~80%) of the whole human FMO3 structure.

Furthermore, that no detectable functional activity of highly purified cDNA expressed FMO3 proteins truncated at several C-terminal positions was observed in this study suggests that the C-terminus of the human FMO3 is important for monooxygenation action. Taken together with the present results, the Cys197stop FMO3, found in Proband B (Fig. 2), should also be inactive for typical tertiary amine substrates.

The Japanese individuals did not possess any of the previously reported *FMO3* gene mutations that typically cause severe trimethylaminuria symptoms and low metabolic capacity of FMO3 ($\leqslant$40% urinary TMAO formation) [16,19]. We recently reported that relatively low FMO3 metabolic capacity associated with liver damage could be another causal factor for mild trimethylaminuria, independent of the *FMO3* genotype present [32]. On the other hand, the present study is the first report that the stop codons exist as mutants of *FMO3* in Japanese severe trimethylaminuria patients, although further studies are needed to be conducted to clarify whether or not these mutants and/or haplotypes are specific for Japanese suffering from trimethylaminuria. We recently reported two additional missense mutants, Thr201Lys FMO3 and Met260Val FMO3, as a preliminary single nucleotide polymorphism communication [28] from DNA of the other three subjects in this Japanese cohort showing less than 40% FMO3 metabolic capacities. Although these variants have not been fully characterized yet in terms of FMO3 function, recombinant Thr201Lys FMO3 and Met260Val FMO3 expressed in the bacterial membranes had impaired catalytic function in our preliminary study. Recently reported *FMO3* upstream variant haplotypes [33] and/or alternative processing [34] might also contribute to decreased *FMO3* expression and incidence of trimethylaminuria. Regardless, the present results suggest that truncation mutations of the *FMO3* gene that result in stop codons might be one of the causes of fish-like odor syndrome or trimethylaminuria in a Japanese cohort suffering from self-reported malodor, albeit at low frequencies (~2–4%). The frequency of these mutations should be low in healthy Japanese populations because they could not be found at all in approximately 100 alleles tested in control individuals (data not shown). The results from the present study also suggest that harboring at least one wild-type or decreased but not inactive allele of the *FMO3* gene could have FMO3 metabolic capacity and this may be relevant to diagnosis of trimethylaminuria.

In conclusion, individuals homozygous for either of the nonsense mutation Arg500stop or Cys197Stop alleles in the *FMO3* gene can possess abnormal TMA *N*-oxygenation and have trimethylaminuria. Heterozygotes for the nonsense mutations will exhibit trimethylaminuria symptoms only if they have, on the other chromosome, a mutation that substantially impairs enzyme activity (in which case they will have severe trimethylaminuria) or partially impairs enzyme activity (in which case they will have mild trimethylaminuria). The findings of the present study provide fundamental information for the importance of future investigations of the human *FMO3* gene associated with trimethylaminuria (fish-like odor syndrome).

Acknowledgments

We thank all of the volunteers for their participation in this study. We also thank Drs. Masaki Fujieda and Kazuma Kiyotani and Ms. Chihiro Yanagida for their help. This work was supported in part by the Ministry of

Education, Science, Sports and Culture of Japan, The Mochida Memorial Foundation for Medical and Pharmaceutical Research, and Japan Research Foundation for Clinical Pharmacology. J.R.C. was supported financially by a grant from NIH (Grant Number DK 59618).

References

[1] J.R. Cashman, B.R. Akerman, S.M. Forrest, E.P. Treacy, Population-specific polymorphisms of the human FMO3 gene: significance for detoxication, Drug Metab. Dispos. 28 (2000) 169–173.
[2] D.M. Ziegler, An overview of the mechanism, substrate specificities, and structure of FMOs, Drug Metab. Rev. 34 (2002) 503–511.
[3] D. Hernandez, A. Janmohamed, P. Chandan, I.R. Phillips, E.A. Shephard, Organization and evolution of the flavin-containing monooxygenase genes of human and mouse: identification of novel gene and pseudogene clusters, Pharmacogenetics 14 (2004) 117–130.
[4] N. Lomri, Q. Gu, J.R. Cashman, Molecular cloning of the flavin-containing monooxygenase (form II) cDNA from adult human liver, Proc. Natl. Acad. Sci. USA 89 (1992) 1685–1689.
[5] J. Zhang, J.R. Cashman, Quantitative analysis of FMO gene mRNA levels in human tissues, Drug Metab. Dispos. 34 (2006) 19–26.
[6] L.H. Overby, G.C. Carver, R.M. Philpot, Quantitation and kinetic properties of hepatic microsomal and recombinant flavin-containing monooxygenases 3 and 5 from humans, Chem. Biol. Interact. 106 (1997) 29–45.
[7] S.B. Koukouritaki, P. Simpson, C.K. Yeung, A.E. Rettie, R.N. Hines, Human hepatic flavin-containing monooxygenases 1 (*FMO1*) and 3 (*FMO3*) developmental expression, Pediatr. Res. 51 (2002) 236–243.
[8] D. Hernandez, S. Addou, D. Lee, C. Orengo, E.A. Shephard, I.R. Phillips, Trimethylaminuria and a human *FMO3* mutation database, Hum. Mutat. 22 (2003) 209–213.
[9] J. Zhang, Q. Tran, V. Lattard, J.R. Cashman, Deleterious mutations in the flavin-containing monooxygenase 3 (*FMO3*) gene causing trimethylaminuria, Pharmacogenetics 13 (2003) 495–500.
[10] S.B. Koukouritaki, R.N. Hines, Flavin-containing monooxygenase genetic polymorphism: impact on chemical metabolism and drug development, Pharmacogenomics 6 (2005) 807–822.
[11] S.C. Mitchell, R.L. Smith, Trimethylaminuria: the fish malodor syndrome, Drug Metab. Dispos. 29 (2001) 517–521.
[12] J.R. Cashman, J. Zhang, Interindividual differences of human flavin-containing monooxygenase 3: genetic polymorphisms and functional variation, Drug Metab. Dispos. 30 (2002) 1043–1052.
[13] E.P. Treacy, B.R. Akerman, L.M. Chow, R. Youil, C. Bibeau, J. Lin, A.G. Bruce, M. Knight, D.M. Danks, J.R. Cashman, S.M. Forrest, Mutations of the flavin-containing monooxygenase gene (*FMO3*) cause trimethylaminuria, a defect in detoxication, Hum. Mol. Genet. 7 (1998) 839–845.
[14] J.R. Cashman, K. Camp, S.S. Fakharzadeh, P.V. Fennessey, R.N. Hines, O.A. Mamer, S.C. Mitchell, G. Preti, D. Schlenk, R.L. Smith, S.S. Tjoa, D.E. Williams, S. Yannicelli, Biochemical and clinical aspects of the human flavin-containing monooxygenase form 3 (FMO3) related to trimethylaminuria, Curr. Drug Metab. 4 (2003) 151–170.
[15] S.C. Mitchell, Trimethylaminuria: susceptibility of heterozygotes, Lancet 354 (1999) 2164–2165.
[16] J. Zschocke, D. Kohlmueller, E. Quak, T. Meissner, G.F. Hoffmann, E. Mayatepek, Mild trimethylaminuria caused by common variants in *FMO3* gene, Lancet 354 (1999) 834–835.
[17] C.T. Dolphin, A. Janmohamed, R.L. Smith, E.A. Shephard, I.R. Phillips, Missense mutation in flavin-containing mono-oxygenase 3 gene, *FMO3*, underlies fish-odour syndrome, Nat. Genet. 17 (1997) 491–494.
[18] J.R. Cashman, Human flavin-containing monooxygenase (form 3): polymorphisms and variations in chemical metabolism, Pharmacogenomics 3 (2002) 325–339.
[19] J.R. Cashman, The implications of polymorphisms in mammalian flavin-containing monoloxygenases in drug discovery and development, Drug Discov. Today 9 (2004) 574–581.
[20] M. Fujieda, H. Yamazaki, M. Togashi, T. Saito, T. Kamataki, Two novel single nucleotide polymorphisms (SNPs) of the *FMO3* gene in Japanese, Drug Metab. Pharmacokinet. 18 (2003) 333–335.
[21] A. Brunelle, Y.A. Bi, J. Lin, B. Russell, L. Luy, C. Berkman, J. Cashman, Characterization of two human flavin-containing monooxygenase (form 3) enzymes expressed in *Escherichia coli* as maltose binding protein fusions, Drug Metab. Dispos. 25 (1997) 1001–1007.
[22] H. Yamazaki, M. Fujieda, M. Togashi, T. Saito, G. Preti, J.R. Cashman, T. Kamataki, Effects of the dietary supplements, activated charcoal and copper chlorophyllin, on urinary excretion of trimethylamine in Japanese trimethylaminuria patients, Life Sci. 74 (2004) 2739–2747.
[23] M. Kubota, Y. Nakamoto, K. Nakayama, P. Ujjin, S. Satarug, T. Mushiroda, T. Yokoi, M. Funayama, T. Kamataki, A mutation in the flavin-containing monooxygenase 3 gene and its effects on catalytic activity for *N*-oxidation of trimethylamine*in vitro*, Drug Metab. Pharmacokinet. 17 (2002) 207–213.
[24] A.Q. Zhang, S. Mitchell, R. Smith, Fish odour syndrome: verification of carrier detection test, J Inherit. Metab Dis. 18 (1995) 669–674.
[25] B. Richards, J. Skoletsky, A.P. Shuber, R. Balfour, R.C. Stern, H.L. Dorkin, R.B. Parad, D. Witt, K.W. Klinger, Multiplex PCR amplification from the CFTR gene using DNA prepared from buccal brushes/swabs, Hum. Mol. Genet. 2 (1993) 159–163.
[26] E.J. Faeder, L.M. Siegel, A rapid micromethod for determination of FMN and FAD in mixtures, Anal. Biochem. 53 (1973) 332–336.
[27] V. Lattard, J. Zhang, Q. Tran, B. Furnes, D. Schlenk, J.R. Cashman, Two new polymorphisms of the *FMO3* gene in Caucasian and African-American populations: comparative genetic and functional studies, Drug Metab. Dispos. 31 (2003) 854–860.
[28] M. Shimizu, H. Fujita, T. Aoyama, H. Yamazaki, Three novel single nucleotide polymorphisms of the *FMO3* gene in a Japanese population, Drug Metab. Pharmacokinet. 21 (2006) 245–247.
[29] C.T. Dolphin, J.H. Riley, R.L. Smith, E.A. Shephard, I.R. Phillips, Structural organization of the human flavin-containing monooxygenase 3 gene (FMO3), the favored candidate for fish-odor syndrome, determined directly from genomic DNA, Genomics 46 (1997) 260–267.
[30] M.P. Lawton, R.M. Philpot, Functional characterization of flavin-containing monooxygenase 1B1 expressed in *Saccharomyces cerevisiae* and *Escherichia coli* and analysis of proposed FAD- and membrane-binding domains, J. Biol. Chem. 268 (1993) 5728–5734.
[31] S. Eswaramoorthy, J.B. Bonanno, S.K. Burley, S. Swaminathan, Mechanism of action of a flavin-containing monooxygenase, PNAS 103 (2006) 9832–9837.
[32] H. Yamazaki, M. Fujieda, J.R. Cashman, T. Kamataki, Mild trimethylaminuria observed in a Japanese cohort with liver damage, Am. J. Med. 118 (2005) 803–805.
[33] S.B. Koukouritaki, M.T. Poch, E.T. Cabacungan, D.G. McCarver, R.N. Hines, Discovery of novel flavin-containing monooxygenase 3 (FMO3) single nucleotide polymorphisms and functional analysis of upstream haplotype variants, Mol. Pharmacol. 68 (2005) 383–392.
[34] V. Lattard, J. Zhang, J.R. Cashman, Alternative processing events in human *FMO* genes, Mol. Pharmacol. 65 (2004) 1517–1525.

Available online at www.sciencedirect.com
ScienceDirect
Biochemical and Biophysical Research Communications 352 (2007) 514–521
BBRC
www.elsevier.com/locate/ybbrc

Proteomics-based identification of biomarkers for predicting sensitivity to a PI3-kinase inhibitor in cancer

Tetsuyuki Akashi [a], Yumiko Nishimura [a], Rumi Wakatabe [b], Mieko Shiwa [b], Takao Yamori [a,*]

[a] *Division of Molecular Pharmacology, Cancer Chemotherapy Center, Japanese Foundation for Cancer Research, 3-10-6 Ariake, Koto-ku, Tokyo 135-8550, Japan*

[b] *Yokohama Laboratory, Ciphergen Biosystems K. K., Yokohama Business Park East Tower 14F, 134 Godo-cho, Hodogaya-ku, Yokohama, Kanagawa 240-0005, Japan*

Received 25 October 2006
Available online 20 November 2006

Abstract

To identify biomarkers for predicting sensitivity to phosphatidylinositol 3-kinase (PI3K) inhibitors, we have developed a proteomics-based approach. Using surface-enhanced laser desorption-ionization time-of-flight mass spectrometry (SELDI-TOF MS), we measured the expression of 393 proteins in 39 human cancer cell lines (JFCR-39), and combined it with our previously established chemosensitivity database to select for proteins whose expressions show significant correlations to drug sensitivities. This integrated approach allowed us to identify peaks from two proteins, 11.6 and 11.8 kDa, that showed significant correlations with the sensitivity to a PI3K inhibitor, LY294002. We found that the 11.8 kDa protein was a phosphorylated form of the 11.6 kDa protein. While the 11.8 kDa protein showed a positive correlation with the sensitivity to LY294002, the 11.6 kDa protein showed a negative correlation with that of the LY294002. The 11.6 kDa protein was purified chromatographically, and was identified by SELDI-TOF MS as the ribosomal P2 protein, which possesses two prospective phosphorylation sites. These results suggested that the phosphorylation status of the ribosomal P2 was responsible for determining the sensitivity to LY294002, and that the ribosomal P2 could be a potential biomarker for predicting chemosensitivity.

Keywords: SELDI-TOF MS; Proteomics; Biomarker; Prediction of chemosensitivity; Phosphorylation; Ribosomal P2

Characteristics of cancer cells vary from patients to patients, as they are transformed from various tissues and many types of physiological disorders contribute to their progress. Such variations cause differential response to anti-cancer drugs, thus resulting in a diversity of chemosensitivity in cancer cells. Accurate prediction of chemosensitivity in cancer therapy is particularly desirable in the clinic to avoid toxic side effects and to eliminate the use of any ineffective agent. Therefore, new biomarkers for predicting chemosensitivity are highly sought after to improve the current clinical capabilities, and the methodologies for the identification of potential biomarkers are in demand.

Panels consisting of human cancer cell lines coupled to a drug activity database are good models for investigating the diversity of chemosensitivity in cancer cells [1–3]. We have established a panel of 39 human cancer cell lines (termed JFCR-39 lines), and used this panel of cells to demonstrate that it provides a powerful means to predict the mechanism of drug action and identify new target compounds. For example, such integrative approaches have led to the identification of MS-247 [4], FJ5002 [5], and ZSTK474 [6] as target compounds for the topoisomerase I/II, telomerase, and phosphatidylinositol 3-kinase (PI3K), respectively. In addition, the panel of cells was used in combination with an array-based gene expression database to identify gene biomarker candidates for the prediction of chemosensitivity [7,8]. However, despite

* Corresponding author. Fax: +81 3 3570 0484.
E-mail address: yamori@jfcr.or.jp (T. Yamori).

0006-291X/$ - see front matter © 2006 Elsevier Inc. All rights reserved.
doi:10.1016/j.bbrc.2006.11.052

providing valuable and comprehensive data, the gene expression analysis method was not very useful in revealing any information on the post-translational modifications (such as phosphorylation, processing, glycosylation, acetylation, methylation, etc.) of the encoded proteins.

The recent development of proteomics-based technology has provided many tools for analyzing proteins from crude cell extracts. These new tools are expected to overcome the problem associated with the gene expression analysis technique. One such technology is surface-enhanced laser desorption-ionization time-of-flight mass spectrometry (SELDI-TOF MS). This technology uses protein chips made of a variety of chromatographic surfaces to selectively retain proteins from crude extracts, and provides a peak whose intensity is relatively quantitative and reproducible measure of a particular protein [9,10].

Our long-term goal is to identify protein biomarkers for predicting sensitivity to anti-cancer drugs. To identify the biomarkers, we comprehensively measured protein expression in the JFCR-39 lines by using the proteomics tool, SELDI-TOF MS, and combined it with our previous chemosensitivity database [3,4,6] to select proteins whose expressions show significant correlations to drug sensitivities. In the present study, we focused on LY294002 [11], one of the PI3K inhibitors, as a model of molecular-targeted drugs. The PI3K pathway is frequently activated in various types of cancer cells, and is believed to promote cell proliferation, growth, and survival [12,13]. Therefore, drugs targeted to PI3K are expected to be one of the efficient anti-cancer drugs [14,15]. Recently, several PI3K inhibitors have been developed for this purpose [6,16]. However, useful biomarkers determining chemosensitivity to PI3K inhibitors are currently unknown.

Here we report the finding of a biomarker candidate for the PI3K inhibitor LY294002 from an integrated database, and have identified the biomarker as the ribosomal P2 protein. Simultaneously, we have demonstrated that the SELDI-TOF MS can be used to isolate phosphoproteins from crude cell extracts. The identified ribosomal P2 may serve as a tool for predicting chemosensitivity.

Materials and methods

Cell lines and cell culture. The JFCR-39 [3] lines, used in this study, consist of the following 39 cancer cells: lung cancer, NCI-H23, NCI-H226, NCI-H522, NCI-H460, A549, DMS273, and DMS114; colorectal cancer, HCC-2998, KM-12, HT-29, HCT-15, and HCT-116; gastric cancer, St-4, MKN-1, MKN-7, MKN-28, MKN-45, and MKN-74; breast cancer, HBC-4, BSY-1, HBC-5, MCF-7, and MDA-MB-231; ovarian cancer, OVCAR-3, OVCAR-4, OVCAR-5, OVCAR-8, and SK-OV-3; glioma, U251, SF-268, SF-295, SF-539, SNB-75, and SNB-78; renal cancer, RXF-631L and ACHN; melanoma, LOX-IMVI; and prostate cancer, DU-145 and PC-3. All cell lines were cultured in RPMI 1640 supplemented with 5% fetal bovine serum, penicillin (100 U/ml), and streptomycin (100 μg/ml) at 37 °C in humidified air containing 5% CO_2.

Sample preparation for protein expression database. Cells were seeded at 1×10^6–6.8×10^6 cells in 100-mm dish and grown for 48 h at 37 °C. Cells were washed three times with cold PBS, scraped off the plate, and frozen in liquid N_2. Each frozen cell pellet was suspended in 800 μl of lysis buffer (50 mM Hepes–NaOH, pH 7.5, 0.5% Nonidet P-40, 1 mM sodium orthovanadate, 25 mM sodium fluoride, 15 mM pyrophosphate, and 5 mM EDTA) containing protease inhibitors (0.1 mM phenylmethylsulfonyl fluoride, 1 μg/ml leupeptin, and 1 μg/ml pepstatin) and incubated on ice for 30 min. After centrifugation at 20,000*g* for 20 min, the proteins in the supernatant were denatured by addition of solid urea, CHAPS, and DTT at the final concentration of 6 M, 2%, and 1 mM, respectively. Protein concentration was estimated using a Protein Assay Kit (Bio-Rad, Hercules, CA, USA) and adjusted to 1 mg/ml. All samples were stored at −80 °C.

Protein expression analysis on protein chips and data processing. Protein expression database of the samples was obtained by using strong anion-exchange (Q10), weak cation-exchange (CM10), immobilized affinity capture (IMAC30) charged with Ni^{2+} of protein chips (Ciphergen Biosystems, Fremont, CA, USA). Using a 96-well type bioprocessor, chips were pre-equilibrated two times with 200 μl of an appropriate binding buffer as follows: Q10 chip with 0.1 M Hepes–NaOH, pH 8.0, or 0.1 M sodium acetate, pH 5.0; CM10 chip with 0.1 M sodium phosphate, pH 7.0, or 0.1 M sodium acetate, pH 4.0; and IMAC30 chip with PBS. Each sample was diluted 1:1 in one of the binding buffers to 0.5 mg/ml and 50 μl of the diluted sample was applied to the respective chip. After incubation for 15 min at room temperature, the chips were washed three times with 200 μl of the respective binding buffer for 5 min and rinsed once with 200 μl of deionized water. Spots on the chips were allowed to dry, and each spot was twice treated with 0.5 μl of saturated sinapinic acid (SPA) or α-cyano-4-hydroxy cinnamic acid (CHCA) in 50% acetonitrile in water containing 0.5% trifluoroacetic acid. The protein chips were analyzed using the ProteinChip Biology System Reader (Model PBS II, Ciphergen) and the data were analyzed by ProteinChip Software version 3.2 (Ciphergen). All data were normalized using total ion current normalization function of the software.

Correlation analysis between protein expression and chemosensitivity databases. The chemosensitivity database was obtained by determining the 50% growth inhibition parameter (GI_{50}) for each drug as described previously [4,7]. The degree of correlation between the protein expression and drug activity was calculated using the following Pearson correlation coefficient formula: $r = \sum x_i(y_i - y_m)/\{\sum x_i^2(y_i - y_m)^2\}^{1/2}$, where x_i represents the expression of protein (peak intensity value) in cell i, y_i is the log sensitivity ($|\log_{10}GI_{50}|$) of cell i to drug y, and y_m represents the mean sensitivity ($|\log_{10}GI_{50}|$) of the drug. In this analysis, we selected the protein peak that passed the cut-off filter (peak intensity signal:noise ratio >10). We then selected the peaks where the protein expression patterns showed significant correlations to the drug activity patterns. A significant correlation was defined as having a $P < 0.005$ and a correlation coefficient $>|0.4|$.

Phosphatase treatment. Cells (A549), grown as above in 100-mm dish, were washed three times in cold PBS, scraped off from the dish, and then frozen in liquid N_2. The cell pellet was suspended in 800 μl of lysis buffer (50 mM Hepes–NaOH, pH 7.5, 0.5% Nonidet P-40) containing protease inhibitors (0.1 mM phenylmethylsulfonyl fluoride, 1 μg/ml leupeptin, and 1 μg/ml pepstatin) and incubated on ice for 30 min. After centrifugation at 20,000*g* for 20 min at 30 °C, the proteins in the supernatant were incubated in the reaction buffer (50 mM Hepes, pH 7.5, 0.1 mM EDTA, 5 mM DTT, and 0.01% Brij 35) with or without lambda protein phosphatase (λ-PPase; New England Biolabs, Beverly, MA, USA). The phosphatase reaction was inhibited by addition of phosphatase inhibitors (1 mM sodium orthovanadate, 25 mM sodium fluoride, and 15 mM pyrophosphate at final concentration).

Purification of biomarker candidates. Cellular proteins from the MKN-1 cells, extracted and denatured as described above, were diluted with an equal volume of the binding buffer (50 mM Hepes–NaOH, pH 7.5, 1 mM sodium orthovanadate, 25 mM sodium fluoride, and 15 mM pyrophosphate) and loaded onto to a Q-Sepharose column (GE Healthcare Bio-Sciences, Piscataway, NJ, USA), which was equilibrated with the same binding buffer. Proteins were eluted with 20 ml of a linear gradient buffer containing increasing NaCl concentration (from 180 to 380 mM) using a flow rate of 1 ml/min, the eluted proteins were collected in 1 ml fractions and were analyzed by SELDI-TOF MS using NP20 chips. Fractions

containing the 11.6, 11.7, and 11.8 kDa protein molecules were further purified using the reverse-phase chromatography on a RPC column (GE Healthcare Bio-Sciences). These proteins were eluted with a 36–40% acetonitrile gradient in 0.05% trifluoroacetic acid using a flow rate of 0.5 ml/min. Eluted proteins were fractionated and analyzed by SELDI-TOF MS using NP20 chips, selected fractions were concentrated using SpeedVac. The concentrated proteins were treated with λ-PPase to dephosphorylate phosphoproteins as described above, and were resolved by 16.5% SDS–PAGE. The gel was analyzed by silver-stain according to a manufacturer's instruction (Daiichi Pure Chemicals, Tokyo, Japan) or was stained with Coomassie brilliant blue to use for the protein identification process as described below.

Identification of biomarker candidates. Gel pieces containing the target 11.6 kDa protein were excised. The gel pieces were sequentially incubated as follows: three times with 50 μl of 50% acetonitrile in 50 mM ammonium bicarbonate, pH 8.0, on a shaker at room temperature for 10 min, one time with 500 μl of 50% acetonitrile in 50 mM ammonium bicarbonate, pH 8.0, for 30 min, and then one time with 50 μl of 100% acetonitrile for 15 min. After the final incubation, the gel pieces were dried by SpeedVac for 15 min. Trypsin (modified, sequencing grade; Roche Diagnostics, Basel, Switzerland) or V8 protease (Roche Diagnostics) in 50 mM ammonium bicarbonate, pH 8.0, was added and incubated for 16 h at 37 °C to digest the C-terminal of Arg/Lys or Glu, respectively. The reaction mixture was applied to NP20 chips and was allowed to air-dry. After drying, 20% saturated CHCA in 50% acetonitrile in water containing 0.5% trifluoroacetic acid was added. To identify the protein, the peptide digests were analyzed both by ProteinChip Biology System for the peptide fingerprint analysis and QSTAR Pulsar i (ABI, Foster, CA, USA) equipped with a PCI 1000 ProteinChip Array interface (Ciphergen) for the sequence tag analysis. Database searches were performed using Mascot search engine (Matrix Science, London, UK).

Results

Protein expression database for 39 human cancer cell lines using SELDI-TOF MS

To measure comprehensive protein expression in the JFCR-39 lines, a series of protein chips were used. The protein expression database was obtained by purification of proteins from each cell lysate using five different conditions (Q10 chip at pH 5.0 and 8.0, CM10 chip at pH 4.0 and 7.0, and IMAC-Ni) and subsequently detected by SELDI-TOF MS using two types of matrices, SPA and CHCA. The SPA was used for the mass-to-charge ratio (m/z) range of 8000–25,000, and the CHCA was used for the m/z range of 3000–10,000. After the acquisition of the protein expression database, we have chosen the protein peaks that passed the cut-off filter (peak intensity signal:noise ratio >10), and selected 393 peaks for further analysis (Supplemental Table 1a–g). The database consisted of the mass and signal intensity values for each peak.

Correlation analysis between protein expression and chemosensitivity databases

To screen for the biomarker candidates determining the chemosensitivity to LY294002, the protein expression database was integrated with the chemosensitivity database that was previously determined by measuring the growth inhibition parameters of LY294002 for the cells in the JFCR-39 lines. The growth inhibition parameter, which indicated sensitivity to the drug, for each cell was defined as the drug concentration (GI_{50}) that inhibits cell growth to 50%. After integration, we performed a correlation analysis between the two databases. For that purpose, we calculated the Pearson correlation coefficients for the 393 protein peaks and sensitivity to LY294002. We then selected the protein peaks that satisfied the following criteria: a significant correlation of $P < 0.005$ and a correlation coefficient of $>|0.4|$. Table 1 lists the 10 protein peaks (m/z), which showed significantly high correlation coefficient values. Notably, the peak with the highest correlation coefficient was the 11.6 kDa peak (11,648 m/z, $r = -0.634$, $P = 0.000015$). The 11.6 kDa protein was purified on a Q10 chip (at pH 8.0 condition) and detected using the SPA as matrix. The two 5.8-kDa peaks showing the second and third highest coefficient values (Table 1) were observed on the same type of chip (Q10). These peaks were considered to be evolved from the doubly charged 11.6 kDa protein. The 11.6 kDa protein peak showed a negative correlation ($r = -0.634$) with the sensitivity to LY294002, suggesting that a cell line expressing higher amounts of 11.6 kDa protein would be more resistant to LY294002 (Fig. 1A).

The raw mass spectrum for the 11.6 kDa peak is shown in Fig. 1B. We also noticed two other peaks, 11.7 kDa (11,729 m/z) and 11.8 kDa (11,808 m/z), respectively, near the 11.6 kDa peak. Interestingly, these two peaks showed a mass difference of 80 and 160 Da, respectively, from that of the 11.6 kDa peak (Fig. 1B). The 80 Da mass difference drew our attention because it is well known that phosphorylation of a peptide leads to an 80 Da shift in mass. Thus, we believe that the 11.7 and 11.8 kDa peaks represent single- and double-phosphorylated forms of the 11.6 kDa protein. More interestingly, the 11.8 kDa protein peak showed a positive correlation ($r = 0.543$, $P = 0.00035$) with the sensitivity to LY294002 (Fig. 1A, Table 1); this is in contrast to that of the 11.6 kDa protein peak, which showed a negative correlation with the sensitivity to LY294002. Taken together, these data suggested that a cell line expressing higher amounts of the 11.8 kDa protein would exhibit

Table 1
List of top 10 protein peaks showing high correlation with the sensitivity to LY294002

No.	m/z	Chip	pH	EAM	r	P
1	11,648	Q10	8	SPA	−0.634	0.000015
2	5827	Q10	8	CHCA	−0.613	0.000034
3	5824	Q10	5	CHCA	−0.562	0.0002
4	11,808	Q10	8	SPA	0.543	0.00035
5	5381	CM10	4	CHCA	−0.525	0.00059
6	3608	CM10	4	CHCA	−0.508	0.00097
7	5906	Q10	8	CHCA	0.499	0.0012
8	5415	CM10	4	CHCA	−0.499	0.0012
9	7130	Q10	8	CHCA	0.495	0.0014
10	7156	Q10	8	CHCA	0.488	0.0016

Note. m/z, chip, pH, EAM, r, and P represents the mass-to-charge ratio of each protein peak, the type of protein chip, pH condition during purification process, the type of matrix for ionization, correlation coefficient, and P value, respectively.

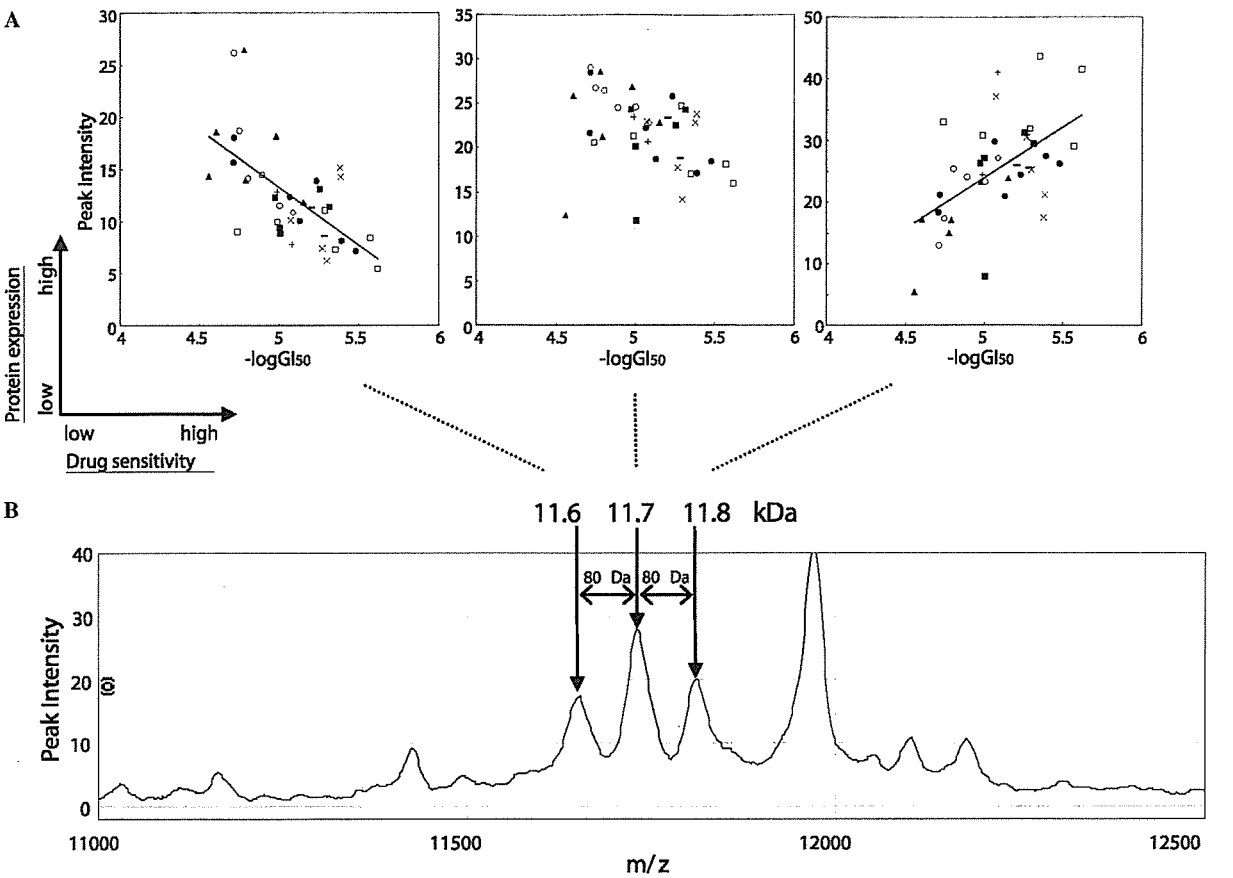

Fig. 1. Selection of target biomarker candidates determining chemosensitivity. (A) Relationship between the expression levels of the three molecules, 11.6 (left), 11.7 (middle), and 11.8 (right) kDa, and chemosensitivity of the JFCR-39 lines to LY294002. The data for each 39 cancer cell line were plotted and were classified using the following different symbols according to their tissue types: lung (●), colon (○), gastric (▲), breast (×), ovarian (■), brain (□), renal (+), melanoma (◇), and prostate (–). The 39 experimental data points were fitted by linear regression analysis. (B) Raw protein expression profile data, including the target peaks. The three target peaks are indicated by arrows. The mass size difference between each target peak was 80 Da.

higher sensitivity to LY294002 than a cell line expressing higher amounts of the 11.6 kDa protein.

SELDI-TOF MS-based analysis for phosphorylated molecules

To verify whether the 11.7 and 11.8 kDa proteins peaks were indeed from two phosphorylated forms of the 11.6 kDa protein, we performed an *in vitro* assay using λ-PPase, which dephosphorylates all types of phosphorylated amino acid residues (i.e., p-Ser, p-Thr, and p-Tyr). Typically, the cellular proteins were incubated with λ-PPase in the absence and presence of phosphatase inhibitors for 60 min at 30 °C, applied to Q10 chips, and then analyzed by SELDI-TOF MS. Results are shown in Fig. 2. The 11.7 and 11.8 kDa peaks clearly disappeared from the reaction mixture treated with λ-PPase (Fig. 2B), but remained in the reaction mixture where the λ-PPase treatment was performed in the presence of the phosphatase inhibitors sodium orthovanadate (1 mM final concentration), sodium fluoride (25 mM final concentration), and pyrophosphate (15 mM final concentration) (Fig. 2C). These results further supported the idea that the 11.7 and 11.8 kDa molecules were single- and double-phosphorylated forms, respectively, of the 11.6 kDa protein.

Protein purification and identification of putative biomarker

To identify the 11.6 kDa protein with two potential phosphorylation sites, the MKN-1 cell lysate, which contained the 11.6, 11.7, and 11.8 kDa proteins in almost equal proportions, was used for large-scale protein purification. In order to monitor the three proteins during the purification process, the protein chips were used. First, we attempted to find an ideal condition to elute three proteins of interest from the Q10 chip using different concentrations of NaCl. We found by SELDI-TOF MS analysis that the targets remained absorbed on the Q10 chip when 200 mM NaCl was used, but were eluted off when 300 mM NaCl was used (data not shown). For large-scale purification, we absorbed cellular proteins, including the targets, onto a Q-Sepharose column and then used a NaCl

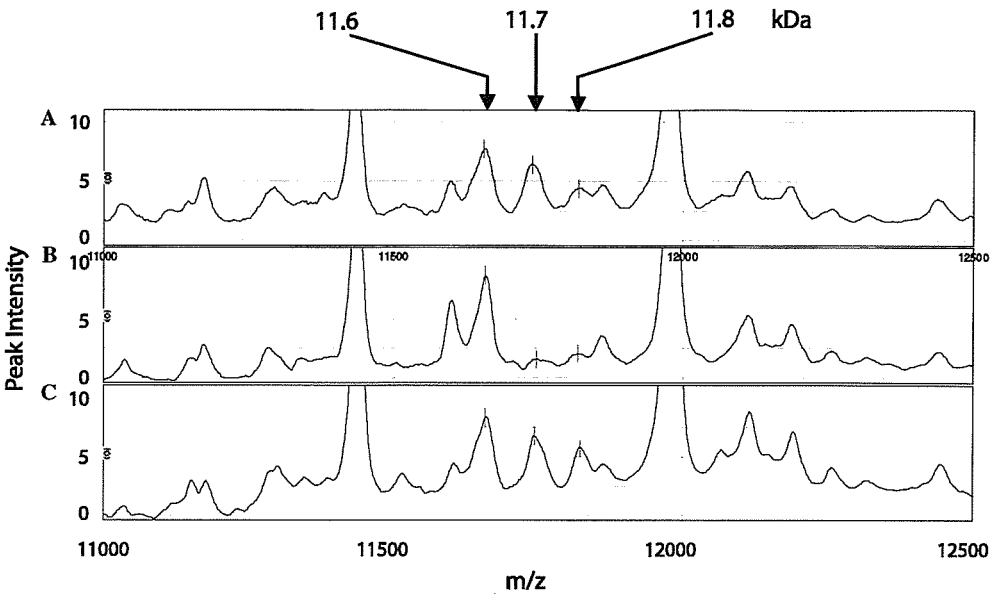

Fig. 2. SELDI-TOF MS-based analysis for determining the phosphorylation status of the target proteins. The cell lysate was incubated with: phosphatase inhibitors (A), λ-PPase (B), and phosphatase inhibitors and λ-PPase (C) for 60 min at 30 °C. Subsequently, each sample was applied to a NP20 chip and was analyzed by SELDI-TOF MS.

concentration gradient from 180 to 380 mM to elute the proteins from the column. Eluted fractions were monitored by SELDI-TOF MS using NP20 chips (Fig. 3A). The pooled fractions containing the target proteins were subjected to reverse-phase chromatography. After adsorption, the proteins were eluted with a 36–40% acetonitrile gradient, and the collected fractions were monitored by SELDI-TOF MS as before (data not shown). Since phosphorylation might inhibit protein digestion, which is necessary for the peptide-mass fingerprinting as described below, these three proteins were first dephosphorylated with λ-PPase. After dephosphorylation, we observed only the 11.6 kDa protein peak by SELDI-TOF MS (Fig. 3B). The 11.6 kDa protein was further purified on a SDS–PAGE (Fig. 3C), then the protein band was digested in-gel with trypsin or V8 protease for generating a peptide map for sequence database integration. The digestion mixture containing the peptides was applied to NP20 chips and analyzed by SELDI-TOF MS. Unique peptide sequences, obtained from the trypsin or V8 protease digestion of the 11.6 kDa protein, were entered into the Mascot search engine. Both search results identified the ribosomal P2 as the top matching protein. The probability scores using the unique fragments from the trypsin and V8 protease digestion were 63 ($P < 0.05$) and 57 ($P < 0.05$), respectively, and the sequence coverage values were 91% and 57%, respectively (data not shown). To further confirm our search results, the trypsin digested 1417.64 *m/z* fragment was analyzed by collision-induced dissociation (CID)-tandem MS with the ProteinChip Interface. We submitted the mass spectra data (masses of the product ions) to database searching using the MS-Tag search engine, and identified the peptide sequence as ILDSVGIEADDDR from the 60S ribosomal P2 (data not shown). The ribosomal P2 is a small (11,665 *m/z*) and acidic (p*I* 4.5) protein, which is consistent with the apparent molecular mass observed by SELDI-TOF MS and binding of the protein onto the Q10 chip that selectively adsorbs proteins with low p*I*s. As expected, the mammalian ribosomal P2 protein was reported to contain two prospective phosphorylation sites (S102 and S105) in the C-terminal region [17,18].

Discussion

In this study, we established a new protein expression database for the JFCR-39 lines by using SELDI-TOF MS, and combined this expression database with our previously determined chemosensitivity database to find novel biomarkers for predicting sensitivity to a PI3K inhibitor, LY294002. By integrating the two databases, we not only identified the chemosensitive biomarker candidate, ribosomal P2, but also discovered that the phosphorylation status of this protein was highly correlated with the sensitivity to LY294002. Furthermore, we demonstrated that the SELDI-TOF MS technology can be successfully utilized to isolate phosphoproteins from crude cell extracts.

The chemosensitivity database contained over 500 chemical compounds, including LY294002, and consisted of anti-cancer drugs and inhibitors [3]. Recently, we used this database to identify an *s*-triazine derivative, ZSTK474, as a novel PI3K inhibitor [6], indicating that the database was reliable and of high quality. Among those hundreds of drugs, the phosphorylation status of the ribosomal P2 also specifically correlated with the sensitivity to other PI3K inhibitors, ZSTK474 and quercetin [19], in a manner similar to that of the LY204002 (data not shown). These

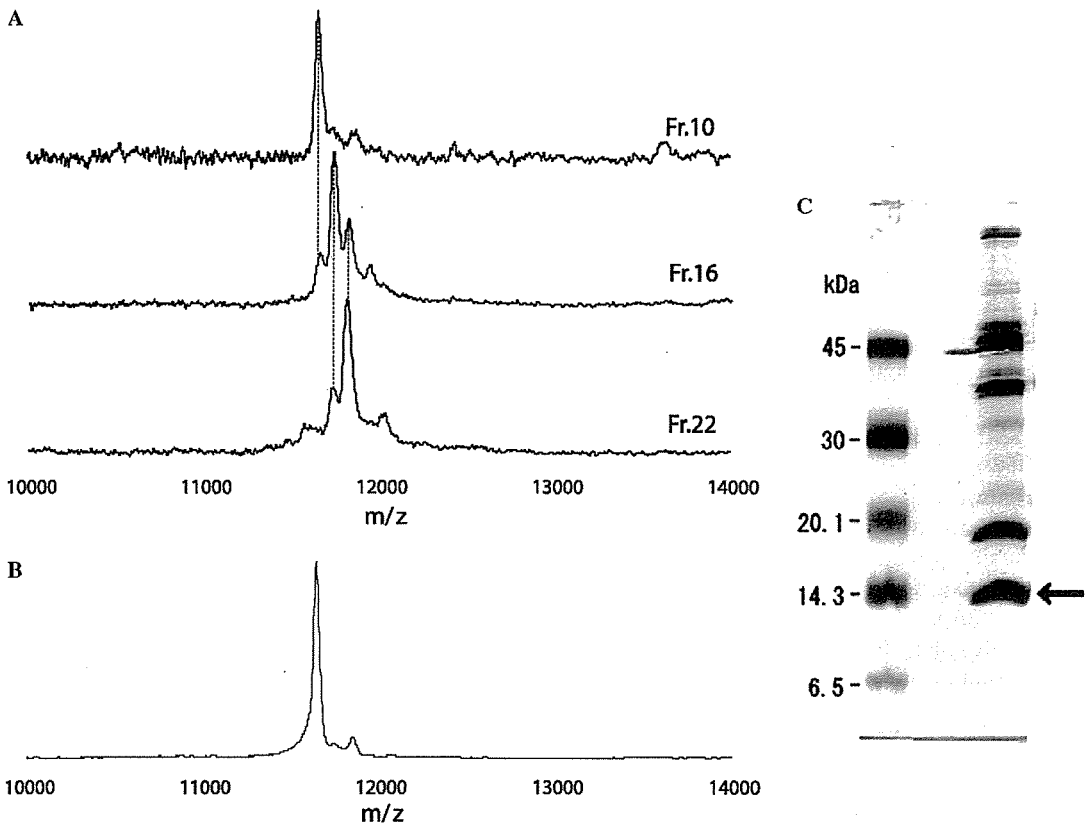

Fig. 3. Purification of the target molecules from the MKN-1 cell lysate. (A) Monitoring of elution during the Q-Sepharose column purification. Proteins from the MKN-1 cell were bound to the Q-Sepharose and eluted at the rate of 1 ml/min with 20 ml of a linear gradient of 180–380 mM NaCl in 50 mM Hepes–NaOH (pH 7.5) buffer containing phosphatase inhibitors. Eluted proteins were collected in 1 ml fractions and analyzed by SELDI-TOF MS using NP20 chips as described in the Materials and methods. Raw mass spectra of fraction numbers 10 (Fr.10), 16 (Fr.16), and 22 (Fr.22) are shown. (B) Dephosphorylation of proteins during the purification process. Proteins were fractionated using the reverse-phase chromatography, and fractions containing the 11.6, 11.7, and 11.8 kDa proteins were concentrated by SpeedVac, treated with λ-PPase, and analyzed by SELDI-TOF MS using NP20 chips. (C) Further purification of the 11.6 kDa protein on a 16.5% SDS–PAGE. The λ-PPase treated proteins were separated by SDS–PAGE and the gel was then silver-stained. The arrow indicates the 11.6 kDa protein band.

results suggested that the phosphorylation status of the ribosomal P2 might be related to the mode of action of the PI3K inhibitors.

Ribosomal P2 is a component of the eukaryotic 60S large ribosomal subunit, which forms a complex with other phosphoproteins (ribosomal P0 and P1 proteins) in the stalk region of the subunit [20]. The mammalian ribosomal P2 possesses two phosphorylation sites (S102 and S105) in the C-terminal region [17,18]. Using reconstituted ribosomes, it was demonstrated that the phosphorylated form of ribosomal P2 remarkably enhanced the protein synthesis *in vitro*, whereas the non-phosphorylated form had no effect on the protein synthesis [17]. It was also demonstrated that a reduction in the ribosomal P2 mRNA level by antisense treatment led to a change in the protein expression pattern compared with the non-treated control [21]. Together, these reports tend to suggest that protein synthesis in cells is controlled by the phosphorylation status of the ribosomal P2, and there might be a relationship between the *in vivo* protein synthesis and the sensitivity to PI3K inhibitors. However, functional significance of the phosphorylation status of the ribosomal P2 is not yet clear. Interestingly, we were able to demonstrate that the phosphorylation status of the ribosomal P2 indeed varied across the 39 cancer cell lines. As described above, cells which were less sensitive to LY294002 expressed a large amount of non-phosphorylated form of the ribosomal P2. Such abundant expression of the non-phosphorylated form of the ribosomal P2 has not been reported elsewhere. Our observations provoked a question whether there is a significant difference in function between the non-phosphorylated and the single- or double-phosphorylated forms of ribosomal P2. It was reported that phosphorylation of the ribosomal P2 increased its affinity for the elongation factor eEF-2, which plays an important role in the translation elongation [22]. Thus, phosphorylation status of ribosomal P2 may play a role in regulating the translation elongation.

The analysis of the regulatory function of phosphorylation might be important in understanding the relationship between the phosphorylation status of ribosomal P2 and the action mode of PI3K inhibitors. It is known that the

phosphorylated ribosomal S6 protein, which is a component of the 40S small ribosomal subunit and is involved in the PI3K signal pathway, efficiently regulated the protein synthesis [23], and PI3K inhibitors blocked this regulatory process [12,14]. However, at present, there is no previous report showing that the ribosomal P2 participates in the PI3K signal pathway. Ribosomal P2 was reported to be phosphorylated *in vitro* by two kinases, casein kinase 2 (CK2) [24] and G protein-coupled receptor kinase 2 (GRK2) [18]. We have found that even though the CK2 activity was strongly inhibited by LY294002 *in vitro* [25], the phosphorylation status of the ribosomal P2 did not change in several cell lines treated with LY294002 (data not shown). Since CK2 phosphorylates numerous substrates [26], implying that it may not a very specific kinase, one cannot exclude the possibility that an alternative kinase or a phosphatase might be involved in regulating the phosphorylation status of the ribosomal P2.

Detecting the phosphoprotein was beyond our expectations. Although mass spectrometry has been used previously to detect purified, phosphorylated small peptides (<5000 m/z) [27] quantitatively, there were few reports describing the detection of phosphoproteins of more than 5000 m/z size from the crude cell extract using mass spectrometry. It has been generally considered that phosphorylation reduces the ionization efficiency of the peptides, and the modified peptides are difficult to detect using mass spectrometry [28]. However, very recently, Le Bihan et al. detected an 18 kDa phosphoprotein by using SELDI-TOF MS [29]. We also successfully detected two phosphorylated forms of 12 kDa ribosomal P2 by SELDI-TOF MS in the present study. These studies may indicate that phosphorylations do not have large effects on the ionization efficiency in SELDI-TOF MS even when phosphoproteins more than 10 kDa are detected. Therefore, SELDI-TOF MS is a powerful tool because not only can it perform proteomic measurements easily, rapidly, and reproducibly [8,9], but also can be used to screen and analyze phosphoproteins from the crude cell extracts.

In conclusion, by combining the two databases we have found a new putative biomarker, ribosomal P2, and demonstrated that the phosphorylation status of ribosomal P2 was responsible for determining the sensitivity to PI3K inhibitors, especially LY294002, in the 39 cancer cell lines. We expect that the phosphorylation status of the ribosomal P2 will be a biomarker for predicting chemosensitivity. Further investigation is required to elucidate the mechanistic link between the phosphorylation status of ribosomal P2 and the chemosensitivity, and to validate this protein as a diagnostic marker.

Acknowledgments

We thank Dr. Shingo Dan for guiding us integrating the two databases. We also thank Kanami Yamazaki, Yoko Yoshida, Seki Mariko, Yumiko Mukai, Mutsumi Okamura for providing the chemosensitivity database, and Miwa Yoshida and Naoto Mitsuhashi for supporting the measurement of the peptide sequence. This work was supported by a grant from National Institute of Biomedical Innovation, Japan, to T. Yamori (05-13); Grants-in-Aid for Scientific Research (B) from Japan Society for the Promotion of Science to T. Yamori (17390032); and Grants-in-Aid of the Priority Area "Cancer" from the Ministry of Education, Culture, Sports, Science and Technology, Japan, to T. Yamori (618).

Appendix A. Supplementary data

Supplementary data associated with this article can be found, in the online version, at doi:10.1016/j.bbrc.2006.11.052.

References

[1] R.H. Shoemaker, The NCI60 human tumour cell line anticancer drug screen, Nat. Rev. Cancer 6 (2006) 813–823.
[2] J.N. Weinstein, T.G. Myers, P.M. O'Connor, S.H. Friend, A.J. Fornace Jr., K.W. Kohn, T. Fojo, S.E. Bates, L.V. Rubinstein, N.L. Anderson, J.K. Buolamwini, W.W. van Osdol, A.P. Monks, D.A. Scudiero, E.A. Sausville, D.W. Zaharevitz, B. Bunow, V.N. Viswanadhan, G.S. Johnson, R.E. Wittes, K.D. Paull, An information-intensive approach to the molecular pharmacology of cancer, Science 275 (1997) 343–349.
[3] T. Yamori, Panel of human cancer cell lines provides valuable database for drug discovery and bioinformatics, Cancer Chemother. Pharmacol. 52 (Suppl. 1) (2003) S74–S79.
[4] T. Yamori, A. Matsunaga, S. Sato, K. Yamazaki, A. Komi, K. Ishizu, I. Mita, H. Edatsugi, Y. Matsuba, K. Takezawa, O. Nakanishi, H. Kohno, Y. Nakajima, H. Komatsu, T. Andoh, T. Tsuruo, Potent antitumor activity of MS-247, a novel DNA minor groove binder, evaluated by an in vitro and in vivo human cancer cell line panel, Cancer Res. 59 (1999) 4042–4049.
[5] I. Naasani, H. Seimiya, T. Yamori, T. Tsuruo, FJ5002: a potent telomerase inhibitor identified by exploiting the disease-oriented screening program with COMPARE analysis, Cancer Res. 59 (1999) 4004–4011.
[6] S. Yaguchi, Y. Fukui, I. Koshimizu, H. Yoshimi, T. Matsuno, H. Gouda, S. Hirono, K. Yamazaki, T. Yamori, Antitumor activity of ZSTK474, a new phosphatidylinositol 3-kinase inhibitor, J. Natl. Cancer Inst. 98 (2006) 545–556.
[7] S. Dan, T. Tsunoda, O. Kitahara, R. Yanagawa, H. Zembutsu, T. Katagiri, K. Yamazaki, Y. Nakamura, T. Yamori, An integrated database of chemosensitivity to 55 anticancer drugs and gene expression profiles of 39 human cancer cell lines, Cancer Res. 62 (2002) 1139–1147.
[8] N. Nakatsu, Y. Yoshida, K. Yamazaki, T. Nakamura, S. Dan, Y. Fukui, T. Yamori, Chemosensitivity profile of cancer cell lines and identification of genes determining chemosensitivity by an integrated bioinformatical approach using cDNA arrays, Mol. Cancer Ther. 4 (2005) 399–412.
[9] M. Shiwa, Y. Nishimura, R. Wakatabe, A. Fukawa, H. Arikuni, H. Ota, Y. Kato, T. Yamori, Rapid discovery and identification of a tissue-specific tumor biomarker from 39 human cancer cell lines using the SELDI ProteinChip platform, Biochem. Biophys. Res. Commun. 309 (2003) 18–25.
[10] M. Moscova, D.J. Marsh, R.C. Baxter, Protein chip discovery of secreted proteins regulated by the phosphatidylinositol 3-kinase pathway in ovarian cancer cell lines, Cancer Res. 66 (2006) 1376–1383.
[11] C.J. Vlahos, W.F. Matter, K.Y. Hui, R.F. Brown, A specific inhibitor of phosphatidylinositol 3-kinase, 2-(4-morpholinyl)-8-phenyl-4*H*-1-benzopyran-4-one (LY294002), J. Biol. Chem. 269 (1994) 5241–5248.

[12] I. Vivanco, C.L. Sawyers, The phosphatidylinositol 3-Kinase AKT pathway in human cancer, Nat. Rev. Cancer 2 (2002) 489–501.
[13] Y. Samuels, K. Ericson, Oncogenic PI3K and its role in cancer, Curr. Opin. Oncol. 18 (2006) 77–82.
[14] J. Luo, B.D. Manning, L.C. Cantley, Targeting the PI3K-Akt pathway in human cancer: rationale and promise, Cancer Cell 4 (2003) 257–262.
[15] L. Stephens, R. Williams, P. Hawkins, Phosphoinositide 3-kinases as drug targets in cancer, Curr. Opin. Pharmacol. 5 (2005) 357–365.
[16] P. Workman, Inhibiting the phosphoinositide 3-kinase pathway for cancer treatment, Biochem. Soc. Trans. 32 (2004) 393–396.
[17] C. Vard, D. Guillot, P. Bargis, J.P. Lavergne, J.P. Reboud, A specific role for the phosphorylation of mammalian acidic ribosomal protein P2, J. Biol. Chem. 272 (1997) 20259–20262.
[18] J.L. Freeman, P. Gonzalo, J.A. Pitcher, A. Claing, J.P. Lavergne, J.P. Reboud, R.J. Lefkowitz, Beta 2-adrenergic receptor stimulated, G protein-coupled receptor kinase 2 mediated, phosphorylation of ribosomal protein P2, Biochemistry 41 (2002) 12850–12857.
[19] W.F. Matter, R.F. Brown, C.J. Vlahos, The inhibition of phosphatidylinositol 3-kinase by quercetin and analogs, Biochem. Biophys. Res. Commun. 186 (1992) 624–631.
[20] M. Remacha, A. Jimenez-Diaz, C. Santos, E. Briones, R. Zambrano, M.A. Rodriguez Gabriel, E. Guarinos, J.P. Ballesta, Proteins P1, P2, and P0, components of the eukaryotic ribosome stalk. New structural and functional aspects, Biochem. Cell Biol. 73 (1995) 959–968.
[21] J. Gardner-Thorpe, H. Ito, S.W. Ashley, E.E. Whang, Ribosomal protein P2: a potential molecular target for antisense therapy of human malignancies, Anticancer Res. 23 (2003) 4549–4560.
[22] P. Bargis-Surgey, J.P. Lavergne, P. Gonzalo, C. Vard, O. Filhol-Cochet, J.P. Reboud, Interaction of elongation factor eEF-2 with ribosomal P proteins, Eur. J. Biochem. 262 (1999) 606–611.
[23] G. Thomas, M. Siegmann, A.M. Kubler, J. Gordon, L. Jimenez de Asua, Regulation of 40S ribosomal protein S6 phosphorylation in Swiss mouse 3T3 cells, Cell 19 (1980) 1015–1023.
[24] P. Hasler, N. Brot, H. Weissbach, A.P. Parnassa, K.B. Elkon, Ribosomal proteins P0, P1, and P2 are phosphorylated by casein kinase II at their conserved carboxyl termini, J. Biol. Chem. 266 (1991) 13815–13820.
[25] S.P. Davies, H. Reddy, M. Caivano, P. Cohen, Specificity and mechanism of action of some commonly used protein kinase inhibitors, Biochem. J. 351 (2000) 95–105.
[26] F. Meggio, L.A. Pinna, One-thousand-and-one substrates of protein kinase CK2? FASEB J. 17 (2003) 349–368.
[27] E. Bowley, E. Mulvihill, J.C. Howard, B.J. Pak, B.S. Gan, D.B. O'Gorman, A novel mass spectrometry-based assay for GSK-3beta activity, BMC Biochem. 6 (2005) 29.
[28] R. Aebersold, M. Mann, Mass spectrometry-based proteomics, Nature 422 (2003) 198–207.
[29] M.C. Le Bihan, Y. Hou, N. Harris, E. Tarelli, G.R. Coulton, Proteomic analysis of fast and slow muscles from normal and kyphoscoliotic mice using protein arrays, 2-DE and MS, Proteomics 6 (2006) 4646–4661.

Special Review

Percellome Projectによる毒性トランスクリプトミクスの新しい試み

Percellome Project as a New Approach to Toxicology Transcriptomics

菅野 純　北嶋 聡　相﨑健一　五十嵐勝秀　中津則之　高木篤也　小川幸男　児玉幸夫

Jun Kanno, Satoshi Kitajima, Ken-ichi Aisaki, Katsuhide Igarashi, Noriyuki Nakatsu, Atsuya Takagi, Yukio Ogawa, Yukio Kodama

身の回りの物質の毒性（有害性）を予測し，その被害を未然に防ぐのが毒性学の役割である．この精度向上を目指したトキシコゲノミクス研究を実施する際に，マイクロアレイなどから細胞１個当たりのmRNAコピー数を得るPercellome法を開発した．90化合物のマウス肝初期応答データを採取し終え，新たな対象（反復投与，胎児毒性，吸入毒性，多臓器連携）を加えたPercellome Projectを展開している．

key words

トキシコゲノミクス，分子毒性学，遺伝子発現カスケード，標準化，Percellome法，３次元多層(Millefeuille) データ

菅野 純　国立医薬品食品衛生研究所 安全性生物試験研究センター 毒性部　E-mail：kanno@nihs.go.jp

1985年東京医科歯科大学大学院医学研究科博士課程修了．人体病理学，実験病理学専攻．国立医薬品食品衛生研究所毒性部室長を経て，2002年より同部長．内分泌かく乱関連などの分子毒性学研究，トキシコゲノミクスプロジェクトなどを厚生労働所掌業務との有機的連携のもとに推進．

北嶋 聡，相﨑健一，五十嵐勝秀，中津則之，高木篤也，小川幸男，児玉幸夫　国立医薬品食品衛生研究所 安全性生物試験研究センター 毒性部

はじめに

医薬品，食品，化粧品，生活関連用品など，身の回りの物質が我々の身体に取り込まれた際に生じる可能性のある毒性（有害性）を予測し，それらの使用に際しての被害を未然に防ぐのが毒性学の役割である[注1]（図1）．具体的には，人々の安全を確保するために使用法（用途）や使用量（残留量）を制限したり，場合によっては禁止したりするための科学的根拠を提供するが，その際，人の身代わりとして実験動物を用いる場合が多い．このような毒性学の精度向上の一環として，従来からの毒性研究（毒性症候学，毒性病理学，など）に加えてのトキシコゲノミクス（Toxicogenomics）研究が進められている．

トキシコゲノミクスでは，物質が生体に及ぼす影響をトランスクリプトームとして観測・解析する．その際，①分子毒性学を構築し種差や個体差の問題，複合暴露の問題などを解決するためには，遺伝子発現カスケードの全容解明を目指す必要がある，②形態学的に変化が現れた段階のトランスクリプトームは，遺伝子発現カスケードの最終段階に過ぎない，③形態変化の現れないごく初期段階を含む遺伝子発現カスケードを描出するためにはまとまった量のデータの蓄積が必須である，との観点から，筆者らは，マイクロアレイや定量PCRから細胞１個当たりのmRNAコピー数を得るPercellome手法と，そのデータ解析のための３次元多層（Millefeuille）システムを開発・実用化した．遺伝子発現量が共通の尺度，すなわち“コピー数／細胞”で表現されることから，検体間，実験間，マイクロアレイのバージョン間，異なったプラットホーム間，などのデータ比較が直接的に行えるようになり，数年かけて蓄積したデータの有機的活用が可能となった．現在，90種類の化学物質によるマウス肝の初期応答データを採取し終えたところである．新たな対象（反復投与，胎児毒性，吸入毒性，多臓器連携）を加えたPercellome Projectの概要を紹介する．

注1　環境への配慮も含まれる．

Ⅰ．Percellome法：細胞１個当たりのmRNA絶対量を得る方法

原理は単純である．サンプルの細胞数を計測し，外部標準mRNA（スパイクRNA）を細胞１個当たり決まった分子数だけそのサンプルに添加し，そしてRNA抽出，測定に移る．サンプルのRNAの測定値を，スパイクRNAの値を基準に，細胞1個当たりのコピー数に換算する．実際には細胞数を直接計測するのが困難なことが多いため，その代替指標として細胞核内のゲノムDNA量を用いる[1), 2)]．定量性・直線性の検証にはLBM標準サンプル（肝[L]と脳[B]を100：0，75：25，50：50，25：75および0：100に混合した5サンプルから成るセット）を用いる．なお，スパイクRNAは，5種類の枯草菌遺伝子のmRNAを濃度公比３で混合したカクテル（dose-graded spike cocktail；GSC）として用意した．高精度を要求されるDNA定量法は手作業プロトコールおよび自動ロボット（PerkinElmer JANUS）のプロトコールを準備